IEEE Access
Multidisciplinary | Rapid Review | Open Access Journal

IEEE Power & Energy Society Section

Received 14 June 2024, accepted 29 July 2024, date of publication 2 August 2024, date of current version 14 August 2024.

Digital Object Identifier 10.1109/ACCESS.2024.3437236

SURVEY

Modeling and Control of Grid Forming Converters: A Systematic Review

MACIT TOZAK[1], (Graduate Student Member, IEEE), SEZAI TASKIN[1], IBRAHIM SENGOR[2], (Senior Member, IEEE), AND BARRY P. HAYES[3,4], (Senior Member, IEEE)

[1]Department of Electrical Electronics Engineering, Manisa Celal Bayar University, 45140 Manisa, Türkiye
[2]Department of Electrical and Electronic Engineering, Munster Technological University, Cork, T12 P928 Ireland
[3]MaREI, the SFI Research Centre for Energy, Climate and Marine, University College Cork, Cork, T23 XE10 Ireland
[4]School of Engineering, University College Cork, Cork, T12 K8AF Ireland

Corresponding author: Barry P. Hayes (barry.hayes@ucc.ie)

ABSTRACT In electrical power systems where the proportion of synchronous generators (SG) is gradually decreasing, grid-forming (GFM) converters need to be installed and controlled to meet all the system requirements that SGs have provided to date. Modeling, control, and implementation of GFM converters have been the subject of numerous studies in recent years, particularly in the context of ensuring grid stability during the transition to non-synchronous renewable energy sources. This paper provides a comprehensive literature review on the modeling and control of grid-connected converters. In particular, the focus is placed on GFM-type control structures, objectives, and applications. Both grid-following (GFL) and GFM control structures are detailed. Then, the objectives of controlling GFM converters in power systems are discussed in detail. Finally, some completed and ongoing GFM installation projects around the world are summarized under the subheadings of battery energy storage system (BESS), GFM wind, hybrid, and high voltage direct current (HVDC).

INDEX TERMS Grid following converter, grid forming converter control, grid forming converter modeling.

I. INTRODUCTION

The global demand for renewable energy sources (RESs) is steadily increasing worldwide to mitigate the growing impacts of climate change. To achieve the goal of transitioning to 100% renewable energy, it is imperative to elevate the proportion of clean energy sources, particularly wind and solar, despite their intermittent nature. Additionally, various energy storage systems (ESSs) will play a crucial role in maintaining the supply-demand balance and system stability. RESs and ESSs are connected to power systems through inverters, and these resources are referred to as inverter-based resources (IBR) [1].

Today, the electrical grid is undergoing a transition from the traditional power system, which relies on large synchronous generators (SGs), to a structure that incorporates a significant number of IBRs. This shift results in a reduction in rotational inertia, which poses challenges for frequency stability and control [2]. On the contrary, power electronic components exhibit fast responsiveness. Therefore, it is envisaged that the difficulties posed by IBRs can be overcome by developing appropriate control methods. That is, the roles currently performed by SGs are expected to be undertaken by IBRs in the future [3]. Furthermore, some calculations and methods developed for SGs will need to be reevaluated for future power systems [4].

The majority of power converters currently used are of the grid following (GFL) type. These converters use the phase-locked loop (PLL) to continuously track the voltage phasor at the point of common coupling (PCC), ensuring that the grid maintains the same voltage magnitude and phase angle. However, a strong network consisting of a high percentage of SGs is needed to maintain the current situation. Otherwise, as the inertia in the system, typically provided by SGs, decreases, maintaining a stable voltage and frequency under disturbances becomes challenging, leading to system

The associate editor coordinating the review of this manuscript and approving it for publication was Guangya Yang.

instability [5]. Hence, advanced converter control methods are required to maintain grid stability and facilitate the utilization of more RESs in future power systems. Especially after the IBR ratio exceeds the 70% range, grid forming (GFM) structures become essential [3]. Converters controlled in GFM mode, which exhibit SG characteristics, have been a focus of interest for both researchers and the industry in recent years.

In this paper, the studies presented as solutions to the above-mentioned problems have been comprehensively reviewed based on GFM control. There are review studies in literature that take into account some aspects of the subject. We categorized review papers on grid-connected GFM converters into four groups. The first group offers a broad perspective on modeling, analysis, or control. The second group evaluates real-world implementations and proposes solutions for utility services. The third group presents specific critical topics pertinent to GFM converters, while the final group delves into exploring various types of a particular GFM control technique. Review articles in the literature are compared with this paper in Table 1 according to control structures, control objectives, and projects.

In the first category, Rosso et al. [6] presented an analysis of control schemes for GFM converters, outlined a generalized control structure, followed by a discussion on some issues, including angle stability, fault ride-through (FRT) capabilities, and the transition from islanded to grid-connected mode. However, GFL methods, system protection, black start, and real-world projects are not investigated. Rathnayake et al. [7] provided an overview of modeling methods, control techniques, protection schemes, applications, and real-world implementations of GFM inverters, yet some topics, such as GFL converters, real-world projects, and some control objectives given in this study are barely addressed. Also, advanced control approaches and many new improvements are not given. Zhang et al. [8] conducted a comparative analysis of GFM control methods and evaluated them based on control structure, grid support capacity, fault current limitation, and stability without touching on advanced control approaches. Xiong et al. [9] surveyed modeling approaches and stability analysis methods for voltage source converter (VSC)-dominated power systems. However, GFL and GFM structures and many control objectives are not included. Gao et al. [5] scrutinized the control architectures of GFL and GFM converters without addressing control objectives and many other issues. Zou et al. [10] investigated the modeling and stability issues of a two-bus electric network incorporating both GFM and GFL converters. Wang et al. [11] presented an overview of synchronization stability for IBRs across diverse grid conditions. Shah et al. [12] reviewed various converter model types and their respective applications. Pishbahar et al. [13] reviewed the stability concepts regarding GFM converters. Liu et al. [14] investigated four AI-based classical grid stability evaluation methods. As given in Table 1, none of these studies address the issue from a broad perspective as given in this study. Since a considerable amount of time has passed since the review studies in this category, and the topic has been extensively studied, many new perspectives are not included in the aforementioned studies, even though some subheadings may be similar. In this study, unlike the above, GFM and GFL control methods are examined in a holistic manner, the explanations are enriched with equations and figures, and the differences between them are pointed out.

In the second category, Shakerighadi et al. [15] provided an overview of the stability challenges surrounding GFM-based IBRs from the perspective of TSOs and vendors. GFM pilot projects and demonstrators installed around the world are reviewed in [16]. Pishbahar et al. [13] also provided some demonstration and pilot projects. Muftau and Fazeli Energy proposed potential solutions influenced by significant academic research and real-world demonstration projects by reviewing virtual synchronous generator (VSG) topologies presented in the literature [17]. Song et al. [18] reviewed GFM inverters, highlighting the potential of GFM technologies in improving power system stability and resilience. However, none of them provide information about the GFM-enabled devices in use and many current projects. In addition, they provide very limited information about advanced control approaches and control objectives.

In the third category, stability challenges are overviewed for power-electronic-dominated power systems considering GFM approaches in [15], Fan et al. [19] provided an overview of current-limiting control methods. Arasteh et al. [20] explored the FRT capability of wind turbines employing various GFM control schemes. Alassi et al. [21] conducted an analysis and comparison of some GFM methods to evaluate their capabilities in generic and soft black-start scenarios. Kkuni et al. [22] conducted a review focused on assessing how the GFC's inner control loops affected their stability under steady-state and large disturbance conditions. However, these studies only review a part of the subject without providing a broad perspective, advanced control approaches, and real-world projects.

In the fourth category, Tayab et al. [23] presented an overview of droop control techniques used to coordinate distributed generation units within microgrids. Chen et al. [24] provided a comparative review of modeling techniques for VSG. Mallemaci et al. [25] conducted a review and comparative analysis of ten of VSG solutions found in the literature, specifically focused on their active power control and inertial capabilities. Cheema reviewed various topologies for virtual inertia and the structure of VSGs, accompanied by an exploration of stability analysis methods like small signal stability and transient stability applied to VSGs [26]. Virtual oscillator control (VOC) based GFM methods were compared according to their oscillator types in [27]. Aghdam and Agamy presented a review of various applications of VOC [28]. Teng et al. [29] offered an introductory overview of GFM control principles and outlined five prevalent control

strategies—droop control, PSC, VSG, direct power control (DPC), and VOC. Vasudevan et al. [30] provided a comprehensive review of synchronverter technology. Nevertheless, these studies do not include all GFM methods, control objectives, and advanced control methods given in this study.

Although modeling and control structures of GFM converters were reviewed broadly in some papers [5], [6], [7], [8], [9], [10], the control objectives have either been superficially explored or not investigated at all. In addition, real-world projects have only been found in [13] and [16], but the list needs to be renewed as the number of applications has increased exponentially recently. Almost none of them offer information about advanced control approaches. This paper contributes to the literature in four ways:

- It provides an up-to-date and comprehensive summary of GFM control.
- It serves as a guide for researchers who want to have a holistic perspective on the control, modeling and analysis of GFM converters.
- The quantities that should be controlled in a converter structure and the properties that are expected from the control are given in detail.
- GFM company products, recently installed and ongoing GFM pilot projects are presented.
- Advanced control techniques associated with the future perspective are also presented.

The literature on grid-connected GFM converters is classified in terms of control perspective. Recent literature on the control, modeling and analysis of GFM converters are examined and grouped under given main headings. Commonly encountered GFM control structures in the literature are examined in Section II. Control objectives are presented in Section III. Real-world completed and ongoing GFM applications in different structures are outlined in Section IV. Suggestions for research directions related to advanced control schemes are given in Section V. Finally, the study is concluded with Section VI.

II. CONTROL STRUCTURES OF SOURCES

Grid-connected converters include different controllers in various structures to regulate injected power, frequency, and voltage. This is realized by taking into account grid codes, which may be different for each country. The primary objective in controller design is to meet the criteria expected by the grid codes on the one hand while ensuring the continuous and stable operation of the converter in both steady-state and transient conditions on the other hand. Various modeling approaches have been proposed in the literature for GFM converters to meet grid requirements. Each of these approaches has its advantages and disadvantages. In this section, converter-based generation units for both GFL and GFM in the literature are classified according to their control structures, as shown in Fig. 1.

In this section, the GFL and GFM control structures are examined. They are utilized to control the grid-connected converter model given in Fig. 2. In the schematic diagram,

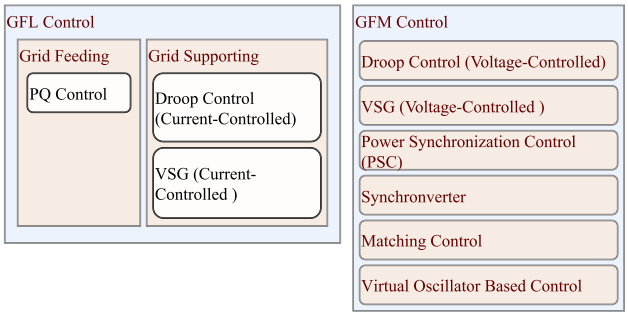

FIGURE 1. Grid connected converter classification according to GFL and GFM control structures.

R_{dc} denotes losses on the DC side of the converter, C_{dc} is the DC link capacitance, and R_f, L_f, and C_f represent filter resistance, inductance, and capacitance, respectively. R_g and L_g are grid-side resistance and inductance. i_{dc} is the DC current supplied by a controllable DC source and v_{dc} is the voltage on the DC link capacitor. $v_{o,abc}$ is the instantaneous voltage in *abc* frame after the switching stage while V_o is the RMS value. $v_{pcc,abc}$ is the filtered voltage at PCC. V_{pcc} is the RMS voltage at PCC. V_g is the RMS value and $v_{g,abc}$ is the instantaneous value of the grid voltage.

A. GRID FOLLOWING (GFL) CONTROL

A GFL converter acts like a current source converter (CSC), consisting of a current source and a parallel high impedance. The simplified model of a GFL converter is given in Fig 3.a.

In GFL control, the measured grid voltage signal is closely tracked by the converter, typically achieved through the PLL device. Presently, this method is employed in most grid-connected converter applications [31].

Active-reactive power (PQ) control is the basic type of GFL control. However, the PQ-controlled converter lacks grid regulation capability and shows limited small-signal stability performance in weak grids [8]. The block diagram of the PQ controller is given in Fig. 4.a. This method attempts to ensure that the active power measurement (P) follows the active power set point (P^{ref}) by regulating the $d-axis$ of the grid current reference ($i_{g,d}^{ref}$). The same method is applied to reactive power set point tracking by arranging the $q-axis$ of grid current reference ($i_{g,q}^{ref}$).

GFL converter strategies such as current-controlled droop [8], [32] and current-controlled VSG [8] could comprise grid-supporting features including (i) steady-state voltage support through reactive power injection, (ii) dynamic voltage support, (iii) FRT, and (iv) primary frequency support in terms of droop and inertia response. Nevertheless, GFL converters may not sustain supporting the grid effectively due to disturbances such as (i) measurement and actuation delay, (ii) weak grid structure caused by the decrease in SG rate and remote connection of an IBR, and (iii) measurement difficulties in PLL and rate of change of frequency (RoCoF) [33]. In the current controlled droop control given in Fig.4.b,

TABLE 1. Comparison of review papers in the recent literature.

Study	Publication Year	Category	Control Structures		Control Objectives									Real-World Projects
			GFM	GFL	C.O.1	C.O.2	C.O.3	C.O.4	C.O.5	C.O.6	C.O.7	C.O.8	C.O.9	
[6]	2021	1	✓		✓	✓	✓	✓	✓				✓	
[7]	2021	1,2	✓	✓	✓	✓		✓	✓	✓	✓		✓	✓
[8]	2021	1	✓	✓	✓	✓		✓	✓	✓				
[9]	2022	1						✓		✓				
[10]	2022	1	✓	✓	✓	✓	✓	✓						
[11]	2020	1	✓	✓		✓	✓	✓						
[12]	2021	1	✓	✓		✓		✓						
[13]	2023	1,2	✓	✓		✓		✓						✓
[14]	2023	1	✓			✓		✓						
[15]	2022	2,3	✓			✓	✓	✓	✓					
[16]	2022	2	✓	✓		✓								✓
[17]	2022	2	✓		✓	✓		✓			✓	✓	✓	✓
[18]	2022	2	✓	✓		✓	✓		✓		✓	✓	✓	✓
[19]	2022	3	✓		✓	✓		✓	✓	✓				
[20]	2022	3	✓			✓			✓					
[21]	2020	3	✓			✓					✓			
[22]	2023	3	✓		✓	✓		✓						
[23]	2017	4	✓		✓	✓								
[24]	2020	4	✓			✓								
[25]	2021	4	✓	✓		✓								
[26]	2020	4	✓			✓		✓						
[27]	2022	4	✓			✓	✓	✓						
[28]	2022	4	✓			✓	✓	✓	✓					
[29]	2022	4	✓	✓		✓								
[30]	2020	4	✓			✓	✓	✓	✓					
This study			✓	✓	✓	✓	✓	✓	✓	✓	✓	✓	✓	✓

C.O.: Control Objective
C.O.1: Device level control
C.O.2: System level control
C.O.3: Grid synchronization
C.O.4: System stability
C.O.5: FRT
C.O.6: System protection
C.O.7: Black start
C.O.8: Seamless transition between GFM and GFL modes
C.O.9: Seamless transition between isolated and grid-connected modes

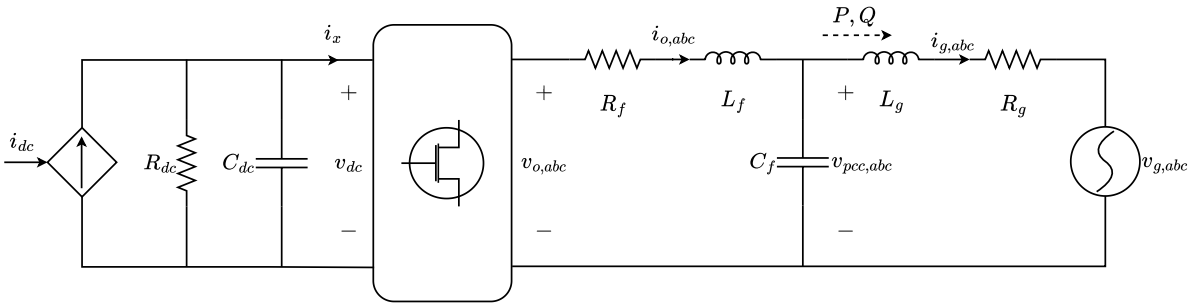

FIGURE 2. Single-line schematic diagram for 3 phase grid-connected converter.

frequency deviation ($\omega^* - \omega$) causes the reference power to change from the operating active power (P_0). ω denotes the measured grid frequency, while ω^* is the reference grid frequency. $K_{\omega P}^{droop}$ is the inverse droop gain which relates frequency deviation with active power change. The Laplace domain control diagram of the current controlled VSG that is based on the swing equation of SG expressed in (1) is given in Fig. 4.c. J is the inertia constant, D_p is the damping coefficient, P_m is the mechanical power, P_e is the electrical power of the machine.

$$J\frac{d\omega}{dt} = P_m - P_e - D_p(\omega - \omega^*) \tag{1}$$

In addition to the methods given above, enhanced GFL control structures based on predictive control [34], table-based direct power control [35], fuzzy logic control [36], repetitive control [37], and neural network-based control [38]

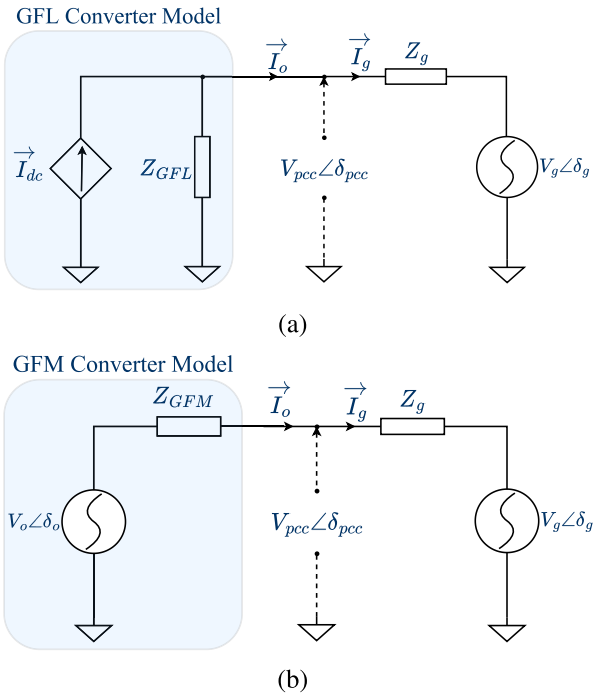

FIGURE 3. Simplified model of (a) GFL and (b) GFM converters.

are also applied to generate current reference signals in the literature.

B. GRID FORMING (GFM) CONTROL

According to North American Electric Reliability Corporation (NERC), *GFM Control for IBRs connected to bulk power systems* is defined as controls designed to keep an internal voltage phasor stable, remaining constant or nearly constant from the sub-transient to transient time frame, [39]. Namely, GFM converters are a type of voltage source converter (VSC). Similar to SGs, they are modeled with a voltage source, represented by the magnitude and phase angle, with a low series impedance. The simplified model of a GFM converter is given in Fig.3.b. The basic principles of commonly used GFM control methods are presented below.

1) DROOP CONTROL

The droop control method, which resembles the speed droop mechanism in SG, is a simple and widely used GFM technique. It ensures synchronization by measuring power imbalance, without PLL, and draws inspiration from the primary frequency control of SG [40]. It has a power-sharing feature proportional to the nominal power of the converter. Droop coefficients are chosen by considering how the converters will share the load according to their rated power in isolated mode [41]. A low pass filter (LPF) is often used in combination with droop control to eliminate high-frequency harmonics from measurements. Notably, droop control relies solely on local measurements and does not necessitate communication between converters. There is an inverse relationship between frequency deviation and power change.

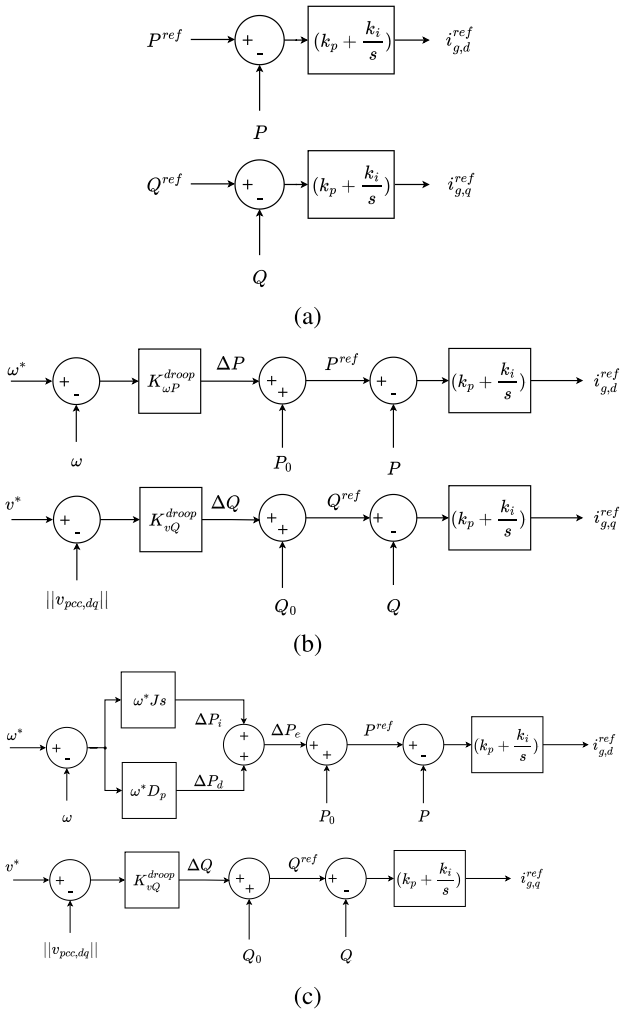

FIGURE 4. Block diagrams for GFL (a) PQ control, (b) current controlled droop, and (c) current controlled VSG methods.

The frequency dynamics of droop control are given in equations (2) and (3). In these equations, θ^{ref} and ω denote the reference angle and angular frequency for the grid voltage, respectively. P signifies measured active power, P^{ref} is the reference active power set point. $K^{droop}_{P\omega}$ represents the droop coefficient, which is calculated as $\frac{\Delta\omega}{S_N}$ where $\Delta\omega$ is the maximum available frequency deviation and S_N is the rated power for the converter [42]. It is also an active power controller (APC), and the terms denoted by "$*$" indicate the nominal values.

$$\dot{\theta}^{ref} = \omega \tag{2}$$

$$\omega = \omega^* + K^{droop}_{P\omega}(P^{ref} - P) \tag{3}$$

The $d-axis$ voltage reference ($v^{ref}_{pcc,d}$) is generated using reactive power – voltage droop property in (4). Here, K^{droop}_{Qv} represents the reactive power controller (RPC) gain and is calculated as $\frac{\Delta V}{S_N}$ where ΔV is the maximum allowable voltage deviation [42]. Frequency control is performed according to (2) and (3), while voltage control is executed based on (4). The block diagrams for these processes are

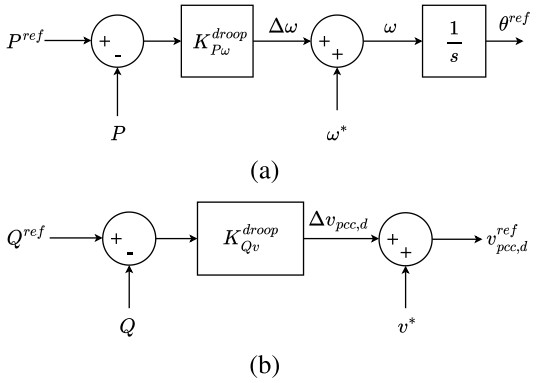

FIGURE 5. Block diagrams for frequency (a) and voltage (b) droop control methods.

provided in Fig.5.a and Fig.5.b, respectively.

$$v^{ref}_{pcc,d} = v^* + K^{droop}_{Qv}(Q^{ref} - Q) \tag{4}$$

2) VIRTUAL SYNCHRONOUS GENERATOR (VSG)

The concept of emulating the behavior of SG with power electronics was first proposed in [43] under the name virtual synchronous machine (VISMA). The VSG concept was proposed in [44], inspired by the swing equation representing the rotor-side dynamics of SG, to stabilize frequency fluctuations in a grid with a predominant presence of IBRs. The frequency dynamics are presented in (5) and (6), and the three-phase voltage induced by the VSG is given in equation (7). The excitation current (i_o) provided in (8) is used to achieve accurate voltage regulation with a PI controller. Therefore, VSG resembles the Automatic Voltage Regulator (AVR) of SG.

$$\dot{\theta}^{ref} = \omega \tag{5}$$

$$\dot{\omega} = \frac{1}{J\omega}\left(P^{ref} - P\right) + \frac{D_p}{J}\left(\omega^* - \omega\right) \tag{6}$$

$$v^{ref}_{pcc,abc} = 2\omega M_f i_o \begin{bmatrix} sin\,(\theta) \\ sin\left(\theta - \frac{2\pi}{3}\right) \\ sin\left(\theta - \frac{4\pi}{3}\right) \end{bmatrix} \tag{7}$$

$$i_o = \frac{k_p}{M_f}\left(v^* - \|v_{pcc,dq}\|\right) + \frac{k_i}{M_f}\int_0^t \left(v^* - \|v_{pcc,dq}(\tau)\|\right) d\tau \tag{8}$$

As the ratio of $\frac{J_r}{D_p}$ approaches 0 in VSG, it resembles droop control. Here, D_p is the damping factor, and J_r represents the virtual rotor's inertia constant. M_f expresses the magnitude of virtual inertia. The block diagrams for VSG control are provided in Fig. 6. VSG-based APC is given in Fig.6.a, the frequency droop characteristic is added in Fig.6.b [45], [46], [81]. The voltage control block diagram is shown in Fig.6.c [4].

There are various enhanced structures of VSG, as seen in [47]. In this example, an adaptive VSG (AVSG) control strategy based on online grid impedance estimation is proposed to ensure robust operation of VSG in both strong and weak grid conditions. VSG control parameters are adjusted based on grid conditions.

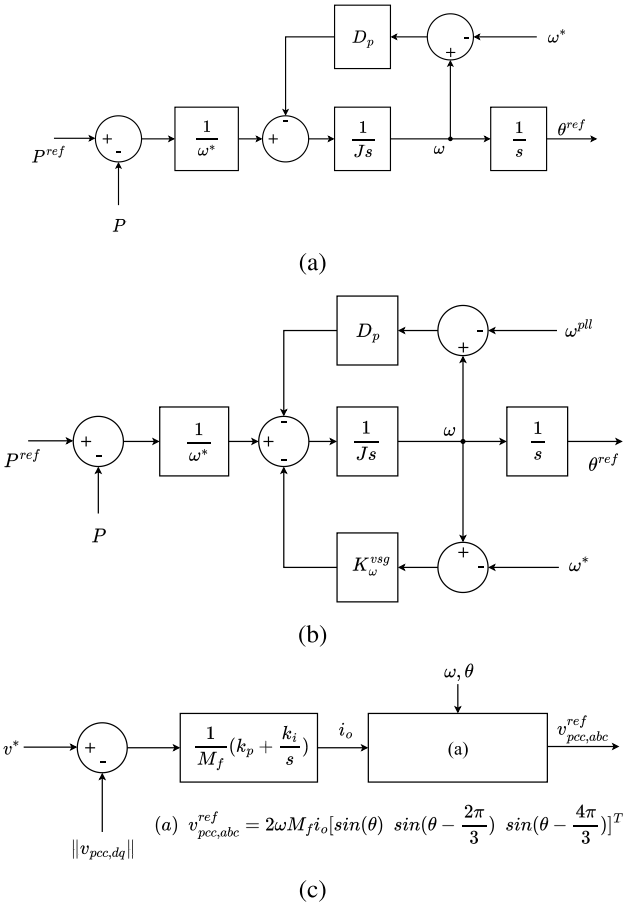

FIGURE 6. VSG control block diagram. (a) VSG-based APC, (b) VSG-based APC with frequency droop characteristic, (c) voltage control.

3) POWER SYNCHRONIZATION CONTROL (PSC)

PSC, the first control method that does not require a synchronization unit, was proposed in [48]. The block diagram of the PSC controlling angle is given in Fig. 7.a and the voltage control is shown in Fig.7.b. The equation for PSC, which mimics the relationship between active power (P) and rotor angle (θ) in SG, is given in equation (9) [49]. In this equation, APC is an integral (I) controller. However, various improved versions of PSC are proposed in the literature. Among these, virtual inertia was achieved in PSC by using a PI controller instead of an I controller [50]. A PSC with both droop and inertia features was designed in [51]. Robust controller design for active power and DC link control gains of PSC was proposed in [52]. The stability boundary and dynamic performance of PSC were assessed based on eigenvalue analysis in weak grids with low SRC in [53].

$$\theta = \theta^{ref} + \frac{K^{PSC}_{P\theta}}{s}\left(P^{ref} - P\right) \tag{9}$$

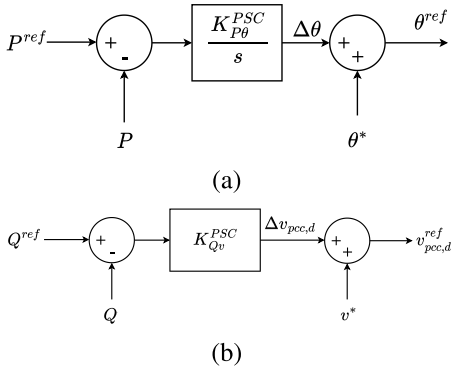

FIGURE 7. PSC block diagram for angle (a) and voltage (b) control.

4) SYNCHRONVERTER

The synchronverter, emulating the behavior of SG, was first proposed in [54]. The block diagram for the synchronverter is provided in Fig. 8 and equations are given in (10), (11), (12), (13), (14), and (15). Here, M_f stands for the mutual inductance between rotor coils and stator coils, and i_f is the excitation current in the rotor.

In [55], the sensitivity of the converter to grid voltage measurement error and processing delay, which cause harmonic distortion, was mitigated by adding fast current loops to the synchronverter. The sensitivity to measurement errors for the 5th order synchronverter model is reduced via virtual output impedance by controlling virtual current in [56]. Synchronverter with FRT capability was proposed to mitigate active and reactive power oscillations, limit excessive currents during faults in [57].

$$\dot{\theta}^{ref} = \omega \tag{10}$$

$$\dot{\omega} = \frac{1}{J}\left(\frac{P^{ref} - P}{\omega^*} - D_P\left(\omega - \omega^*\right)\right) \tag{11}$$

$$v_{pcc,abc}^{ref} = 2\omega M_f i_o \begin{bmatrix} sin\left(\theta\right) \\ sin\left(\theta - \frac{2\pi}{3}\right) \\ sin\left(\theta + \frac{2\pi}{3}\right) \end{bmatrix} \tag{12}$$

$$T_e = M_f i_f \begin{bmatrix} i_{o,a} sin\left(\theta^{ref}\right) \\ i_{o,b} sin\left(\theta^{ref} - \frac{2\pi}{3}\right) \\ i_{o,c} sin\left(\theta^{ref} + \frac{2\pi}{3}\right) \end{bmatrix} \tag{13}$$

$$P = T_e \omega^* \tag{14}$$

$$Q = -\theta^{ref} M_f i_f \begin{bmatrix} i_{o,a} cos\left(\theta^{ref}\right) \\ i_{o,b} cos\left(\theta^{ref} - \frac{2\pi}{3}\right) \\ i_{o,c} cos\left(\theta^{ref} + \frac{2\pi}{3}\right) \end{bmatrix} \tag{15}$$

5) MATCHING CONTROL

Matching control is achieved by matching the deviation in the DC bus voltage of the converter and the power deviation in the electromechanical energy transfer of the SG [58], [59].

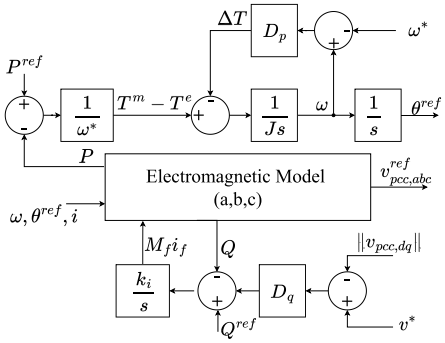

$$(a)\ v_{pcc,abc}^{ref} = \omega M_f i_f [sin(\theta^{ref})\ \ sin(\theta^{ref} - \frac{2\pi}{3})\ \ sin(\theta^{ref} + \frac{2\pi}{3})]^T$$

$$(b)\ P_e = M_f i_f \omega^* [i_{o,a} sin(\theta^{ref})\ \ i_{o,b} sin(\theta^{ref} - \frac{2\pi}{3})\ \ i_{o,c} sin(\theta^{ref} + \frac{2\pi}{3})]^T$$

$$(c)\ Q = -\theta^{ref} M_f i_f [i_{o,a} cos(\theta^{ref})\ \ i_{o,b} cos(\theta^{ref} - \frac{2\pi}{3})\ \ i_{o,c} cos(\theta^{ref} + \frac{2\pi}{3})]^T$$

FIGURE 8. Synchronverter block diagram (adapted from [8]).

The comprehensive electronic implementation of SG and a control design based on energy-shaping techniques were proposed in [60]. Unlike numerical SG emulation methods, it suggests the complete physical implementation of an SG using the integral of the DC bus voltage measurement as the inner angular frequency of the VSC. Matching control establishes an analogy between the physical quantities of SG, such as the moment of inertia and rotor damping coefficient, and those of the VSC. As the input torque of SG is controlled with the output current, it is considered that the DC input current of the converter can be used to control the AC output power. Equation (16) in [4] and (17) in [61] are used to obtain the angle dynamics of the matching control. The k_θ in (16) and (17) represents the ratio of the reference frequency value (ω^*) to the reference DC bus voltage (v_{dc}^*) as given in (18). The magnitude of the AC output voltage is controlled by the modulation signal (μ) obtained by (19). The reference voltage is obtained in the stationary $\alpha\beta$ frame according to (20). The block diagram of the matching control obtained from (16), (18), (19) and (20) is provided in Fig. 9. The disadvantage of matching control is that it manages all control actions, such as DC bus voltage control, grid frequency control, power sharing, and active power control, through a single control gain. This prevents the simultaneous optimization of all functions [62].

$$\dot{\theta}^{ref} = k_\theta v_{dc} \tag{16}$$

$$\dot{\theta}^{ref} = k_\theta (v_{dc} - v_{dc}^*) + \omega^* \tag{17}$$

$$k_\theta := \frac{\omega^*}{v_{dc}^*} \tag{18}$$

$$\mu = k_p \left(v_{pcc}^* - \|v_{pcc,dq}\|\right) + k_i \int_0^t \left(v_{pcc}^* - \|v_{pcc,dq}(\tau)\|\right) d\tau \tag{19}$$

$$v_{pcc,\alpha\beta}^{ref} = \mu \left[-\sin\theta\ \ \cos\theta\right]^T \tag{20}$$

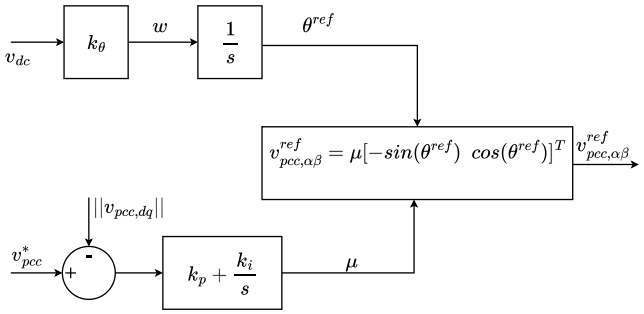

FIGURE 9. Matching control block diagram (adapted from [4]).

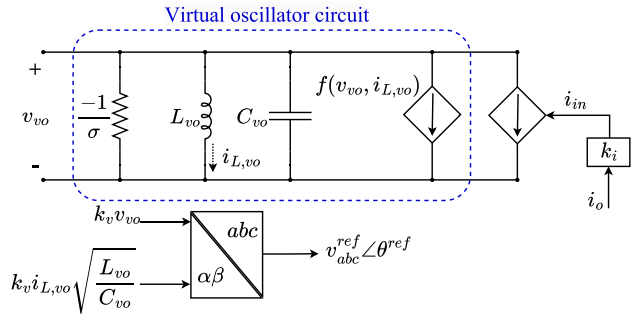

FIGURE 10. Virtual oscillator circuit and VOC based control diagram (adapted from [28]).

6) VIRTUAL OSCILLATOR BASED CONTROL METHODS

Virtual oscillator control (VOC), initially proposed in [63], is a time domain nonlinear control technique that exploits the dynamics of weakly nonlinear oscillator circuits to synchronize converters. Van der Pol, dead-zone, and Andronov-Hopf oscillators were compared in [27] and it was concluded that Andronov-Hopf oscillators are more suitable for grid forming applications because they provide a harmonic free waveform with good dynamic performance. The type of an oscillator is specified with the function $f(v_{vo}, i_{L,vo})$ in Fig. 10. VOC does not involve multiple hierarchical control loops and does not rely on frequency measurement. Therefore, it offers high synchronization and power-sharing speeds [64], [65]. VOC control is designed based on iterative open-loop and full-load tests. During this process, the selected control parameters must meet sufficient conditions for synchronization. The control implementation scheme based on the oscillator is provided in Fig. 10 [27]. The measured output current i_o is used as a feedback signal by multiplying with the current scaling factor k_i.

VOC is a current-controlled voltage source and can not regulate internal voltage directly. So, VOC is augmented in [66] by controlling both current and voltage control with a dual loop-based Andronov Hopf-type oscillator to compensate for voltage deviation.

Dispatchable virtual oscillator control (dVOC), derived from VOC without power dispatchability, was developed in [67] and [68]. The dVOC is a decentralized control strategy that connects an arbitrary number of converters, ensuring

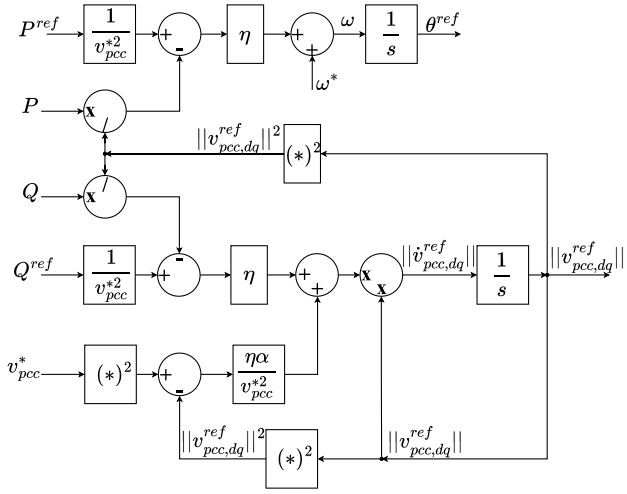

FIGURE 11. Block diagram of dVOC (adapted from [4], [70]).

almost global asymptotic stability based on nominal voltage and power setpoints. The frequency and voltage dynamics of dVOC are presented in (21) and (22) [4]. As it approaches the nominal steady state ($\|v_{pcc,dq}\| \approx v^*_{pcc}$), the relationship between frequency and active power resembles droop control. The block diagram for dVOC generated based on (21) and (22) is provided in Fig. 11. The terms μ and α given in (21) and (22) represent positive control gains.

$$\dot{\theta}^{ref} = \omega^* + \eta\left(\frac{P_{ref}}{v^{*2}_{pcc}} - \frac{P}{\|v^{ref}_{pcc,dq}\|^2}\right) \tag{21}$$

$$\begin{aligned}\|\dot{v^{ref}_{pcc,dq}}\| = {} & \eta\left(\frac{Q^{ref}}{\left(v^*_{pcc}\right)^2} - \frac{Q}{\|v^{ref}_{pcc,dq}\|^2}\right)\|v^{ref}_{pcc,dq}\| \\ & + \frac{\eta\alpha}{\left(v^*_{pcc}\right)^2}\left(\left(v^*_{pcc}\right)^2 - \|v^{ref}_{pcc,dq}\|^2\right)\|v^{ref}_{pcc,dq}\|\end{aligned} \tag{22}$$

Although dVOC offers good synchronization features and power dispatch capability, it does not have effective FRT capacity. Therefore, unified VOC (uVOC) was proposed to effectively overcome the faults. The uVOC strategy can be used as both GFL and GFM and can seamlessly switch between grid-connected and isolated modes in the GFM structure [69].

C. COMPARISON OF GFM CONTROL METHODS

Many GFM control methods are presented in the literature, as explained in the previous section. They have different advantages and disadvantages compared to each other in various situations. Properties, advantages, and limitations of 6 GFM methods and their variations are compared in Table 2.

In the literature and practical applications, the most commonly encountered GFM control methods are droop and

TABLE 2. Performance comparison of GFM control structures.

Method	Topology	Characteristics	Advantages	Limitations
(a) Droop Control	Common features	- Depend on local measurements. - Easy implementation.	- Enhanced small signal frequency stability compared to (e) [74].	- No inertia and damping provision.
	(a1) Single-loop droop control [72]	- Larger coupling reactance. - Angular frequency and inner voltage control.	- Improved dynamic response and stability. - Larger small signal stability boundary compared to (a2).	- Cannot achieve accurate proportional reactive power sharing compared to (a3).
	(a2) Multi-loop droop control [72]	- Inner current and voltage loops. - Angular frequency and capacitor voltage control.	- Voltage and current limits are controlled more tightly compared to (a1).	- Prone to be less damped. - Loses stability more easily compared to (a1).
	(a3) UDE-based robust droop control [73]	- Deals with the model nonlinearity, uncertainty and system disturbances.	- Accurate proportional load sharing among parallel operated inverters.	- Applied only for reactive power regulation.
	(a4) Adaptive droop control [42]	- Adaptively specified droop coefficients according to available power. - Adaptive virtual impedance is used.	- Stably operating and accurately power-sharing with low available power compared to (a1).	- Computational complexity
(b) VSG Control	Common features	- Inertia and damping support. - SG swing equation emulation based.	- Enhanced small signal frequency stability compared to (e) [74].	- Output active power oscillates more than in (a) [77]. - Reduction of provided inertia due to measurement delay [77].
	(b1) VSG	- No need to PLL.	- Lower overshoot and better damping compared to (a2) [45].	- Slower frequency transients compared to (a2) [45].
	(b2) VSG with frequency droop [45], [46], [81]	- PLL measurement is used to implement frequency droop.	- Improve the dynamic response compared to (b1) and (a1) [46]	- Unable to provide adequate voltage support during faults due to the cascaded control [20]
(c) PSC	Common features	- Directly builds a relationship between active power and angle [49]. - Active power balance based synchronization [20].	- More resilient in weak grid connections compared to GFL control [48] - GFL operation with weak grid [69]	- Lack of inertia and damping.
	(c1) PSC with PLL [20]	- Switches to the backup PLL during fault [20].	- Better voltage support during fault than (b2) [20].	- Higher frequency transient during fault than (b2). - More sensitive to power errors than (b2).
	(c2) Robust PSC [52]	- Robust controller design for active power and DC link control gains of PSC	- Suitable for cascaded DC link control to increase stability margin but (b1) is not suitable.	
(d) Synchronverter	Common features [54]	- Mimics the behavior of SG. - Provides damping and inertia.	- Enhanced small signal frequency stability compared to (e) [74].	- Oscillatory power and excessive current injection during fault [57].
	(d1) Synchronverter with fast current loop [55]	- The current loops, compensation of the delays, lead filtered frequency droop, and virtual capacitors	- Reduced sensitivity to measurement errors, processing delay, and grid voltage imbalance.	
	(d2) Virtual impedance based synchronverter [56]	- 5^{th} order synchronverter model. - Controls virtual current flowing through virtual output inductors.	- Reduces sensitivity to measurement errors. [56]. - Limits fault currents and enhances transient stability [127].	
	(d3) Synchronverter with FRT capability [57]	- Two FRT strategies: average and enhanced power control.	- Mitigation of oscillations on powers, excessive current limitation during faults.	
(e) Matching Control	Common features	- Establishes an analogy between the physical quantities of SG. - Inner voltage and current control loops are not needed.	- Enhanced robustness with respect to DC current constraint compared to (a-d) [74].	- Manages all control actions through a single control gain [62].
(f) VOC	Common features	- Time domain method. - Nonlinear control technique that mimics the dynamics of a weakly nonlinear oscillator to synchronize.	- Easy controller implementation compared to (a-d). - Offers high synchronization and power-sharing speed.	- Requires further analysis.
	(f1) Classical VOC [63]	- Load sharing in proportion to converters' ratings. - Current-controlled VSC [66].	- P and Q measurements are not required.	- No power dispatchability - The terminal voltage can not be regulated directly [66].
	(f2) dVOC [67], [68]	- Connects an arbitrarily large number of converters, ensuring almost global asymptotic stability.	- Active and reactive power dispatchability compared to (f1).	- Not effective FRT capability compared to (f3).
	(f3) uVOC [69]	- Operate in both GFL and GFM modes.	- Effective FRT capability compared to (f1,f2). - Seamless transition between grid-connected and islanded modes.	- Vulnerable to asymmetric faults compared to (f4).
	(f4) dsUVOC [76]	- Uses a positive sequence and a negative sequence virtual oscillator.	- Synchronization to fundamental frequency both sequence components - Symmetrical and asymmetrical FRT.	
	(f5) Dual loop based VOC [66]	- Both current and voltage control loops.	- Can regulate internal voltage in case of disturbances compared to (f1).	

VSG control [71]. Various approaches are being developed to improve the dynamic performance of these methods. Conventional droop control is simple and highly flexible but has a slow dynamic response, poor voltage regulation, and poor load-sharing capability [13]. Also, additional inner loops cause the system to lose stability more easily [72]. Therefore, proportional load-sharing and voltage regulation capabilities are improved by robust and adaptive droop control techniques [42], [73].

Droop, VSG, PSC, synchronverter and VOC-based controllers do not consider the DC dynamics of the converter, as the modulation signal is obtained based on only AC-side measurements such as current, voltage, and power flows. Hence, these are called AC-based methods. However, matching control provides information about the dynamics of the DC source. This is called the DC-based method that exhibits robustness against DC source saturation because it takes DC-side measurements into account in angle dynamics. Namely, the matching control is more robust against instability when operating close to current limits of the converter [74].

Droop control, VSG control, PSC, synchronverter and matching control are phasor domain, while VOC-based methods are time domain methods. Although machine-emulation-based phasor domain methods and oscillator-based time domain methods have similar steady-state characteristics, the dynamic characteristics are very different [69]. There is a growing consensus that dVOC is one of the best GFM control methods in terms of performance [27], [75]. VOC-type controllers are easy to implement compared to phasor domain methods including multiple hierarchical control loops. Besides they offer higher synchronization and power-sharing speed. VOC-based methods initially had no dispatchability feature [63]. First, they have gained dispatchability with the dVOC structure [67], [68]. Then, they gain the FRT feature in symmetrical faults with uVOC [69] and in asymmetric faults with dsUVOC [76].

Despite all the valuable improvements, the optimal GFM control method remains an open research topic for the future highly IBR-dominant system [71].

D. COMPARISON OF PHASOR DIAGRAMS OF GFM AND GFL CONVERTERS

A GFL device regulates the transferred power and voltage by controlling the output current of the converter. GFM converters, on the other hand, regulate the output power by directly controlling the terminal voltage. The fundamental difference between GFM and GFL converters lies in their response after a grid event and their small-signal behavior under weak and strong grid conditions [6].

Simplified models of GFL and GFM converters are presented in Fig. 3. The phasor diagram in Fig. 12.a shows the behavior of the GFL converter in response to the disturbance in grid voltage. While maintaining the current phasor (I_g), the voltage phasor of the converter (V_{pcc}) changes. The measured

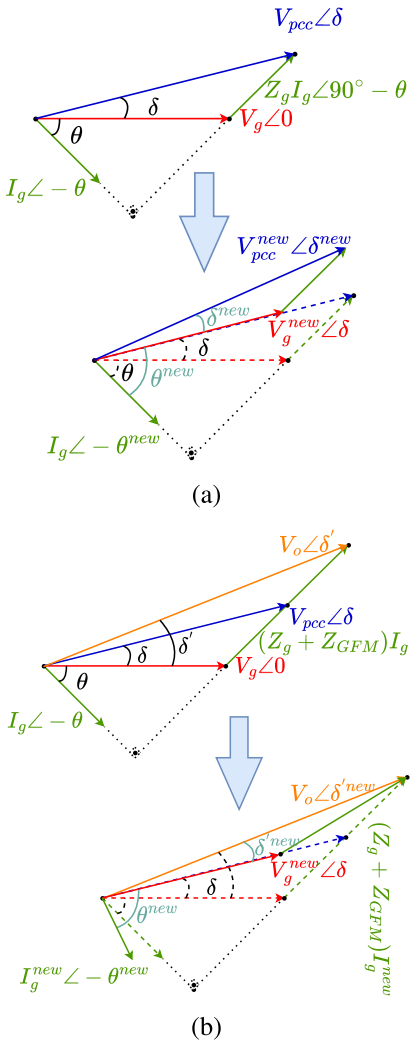

FIGURE 12. Phasor diagrams of (a) GFL and (b) GFM converters under the disturbance on the grid voltage.

grid voltage phase angle (δ^{new}) is required to determine the new current setpoint. The response of the GFM converter after the same event is shown in Fig. 12.b. The internal voltage phasor (V_o) of the converter is initially unaffected by this disturbance. This results in an instantaneous change in the current phasor (I_g) in both magnitude and angle. The rapid increase in converter current could jeopardize the hardware components due to overheating [6].

III. CONTROL OBJECTIVES

NERC recommends that GFM control should provide dynamic supports to the grid such as: (i) operation in weak grids, (ii) stabilizing grid frequency and voltage, (iii) small signal stability damping, (iv) resynchronization capability, (v) FRT and (vi) system restoration and black start [39]. In line with these, this section explores the research on control structures, focusing on which components are targeted for control on the converter and what control actions are applied from a system operator's perspective.

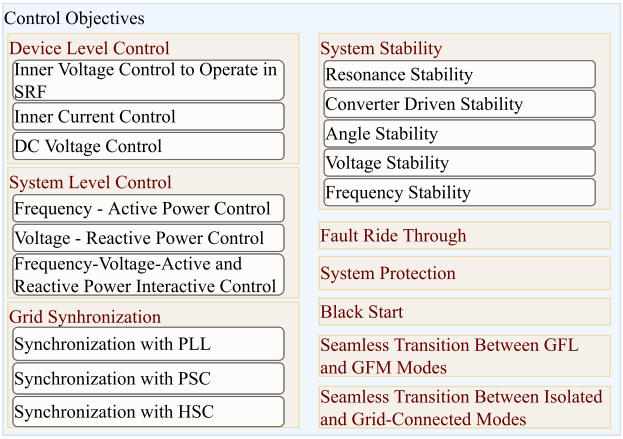

FIGURE 13. Control objectives of GFM converters.

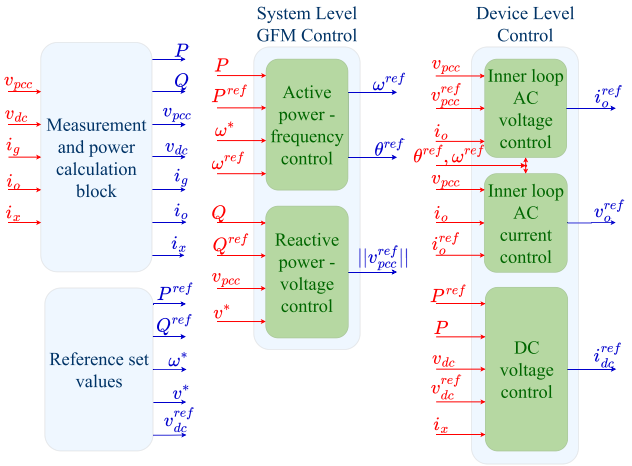

FIGURE 14. Generalized control blocks of GFM converter. (red: input, blue: output).

Two standards that suggest GFM behavior are very important in regulating the connection of IBRs to the grid: IEEE 1547-2018 and IEEE 2800-2022 standards. Minimum technical requirements for the interconnection and interoperability between utility grids and distributed energy resources are regulated by IEEE 1547-2018 standard [78]. Also, minimum technical requirements for the interconnection of IBRs connected to transmission and sub-transmission systems are established in IEEE 2800-2022 standard [79].

Control objectives can be achieved through device- and system-level control, as well as synchronization with the grid. The control scheme of VSCs consists of two control layers, which are device-level control and system-level control. The internal control loops (device-level) use reference signals (voltage, frequency, phase angle, etc.) from the external control loops (system-level) [70]. One of the control objectives is to ensure synchronization of the source with the grid, while another crucial aspect is to ensure stability. Additionally, some system support functions, such as FRT, system protection, and black start are important goals. Subsections that cover the literature regarding the control objectives of the GFM converters are provided in Fig. 13.

The general control structures for GFM converters with multiple loops are provided in Fig. 14. System and device-level control blocks, measurement blocks, and reference signals are explicitly shown in the figure. The converter model is given in Fig. 2. The converter current i_o, grid current i_g, and voltage v_{pcc} are measured. In the outer control loop, phase angle θ^{ref}, frequency ω^{ref}, and voltage magnitude v_{pcc}^{ref} are calculated.

A. DEVICE LEVEL CONTROL

The device-level control, which is given on the right side of Fig. 14, is achieved through inner current and voltage control loops to operate in the synchronous reference frame (SRF) and DC voltage control [80]. Additionally, various current limitation strategies are implemented at this level to prevent instability when operating at current limit values on both the AC and DC sides of the converter. Having open and detailed internal control loops is crucial for addressing and resolving issues related to system-level control design accurately and realistically. The inputs to the device-level inner control loops are voltage, frequency, and phase angle references from the outer loop system-level control, and voltage, current, and power measurements. The virtual impedance block applied at this level will reduce the excessive current and the sensitivity of the converter to small disturbances by readjusting voltage reference coming from system level control. [80], [81].

Device-level control models given below are adapted from [4], [81]. SRF voltage control is implemented using equations (23) and (24). Reference and measured voltages are compared and a current reference is obtained. K_P^V and K_I^V are control gains of the PI controller. K_{ffi} is the feed-forward gain used to enable or disable i_o.

$$\begin{bmatrix} i_{o,d}^{ref\,*} \\ i_{o,q}^{*} \end{bmatrix} = \begin{bmatrix} K_P^V \left(v_{pcc,d}^{ref} - v_{pcc,d} \right) + \\ K_I^V x_{v,d} - C_f . \omega^{ref} . v_{pcc,q} + K_{ffi} . i_{o,d} \\ - \\ K_P^V \left(v_{pcc,q}^{ref} - v_{pcc,q} \right) + \\ K_I^V x_{v,q} + C_f . \omega^{ref} . v_{pcc,d} + K_{ffi} . i_{o,q} \end{bmatrix} \tag{23}$$

$$\begin{bmatrix} \frac{dx_{v,d}}{dt} \\ \frac{dx_{v,q}}{dt} \end{bmatrix} = \begin{bmatrix} v_{pcc,d}^{ref} - v_{pcc,d} \\ v_{pcc,q}^{ref} - v_{pcc,q} \end{bmatrix} \tag{24}$$

The AC current i_o needs to be limited to protect the converter. Equation (25) limits i_o current to i_o^{max} in case of excessive current.

$$\bar{i}_{0,dq}^{ref} \begin{cases} i_{o,dq}^{ref}, & \|i_{o,dq}\| \leq i_o^{max} \\ i_o^{max}, & \|i_{o,dq}\| > i_o^{max} \end{cases} \tag{25}$$

$\bar{i}_o^{ref}$ or i_o^{ref} is compared by i_o and the new voltage reference (v_o^{ref}) is calculated by (26) and (27). K_P^I and K_I^I are control gains of the PI-based current controller. K_{ffv} is the

feed-forward gain factor used to enable or disable v_{pcc}.

$$\begin{bmatrix} v_{o,d}^{ref} \\ v_{o,q}^{ref} \end{bmatrix} = \begin{bmatrix} K_P^I \left(i_{o,d}^{ref} - i_{o,d} \right) + K_I^I . x_{i,d} \\ -L_f . \omega^{ref} . i_{o,q} + K_{ffv} . v_{pcc,d} \\ - - - - - - - - - - - - - - - - - - - \\ K_P^I \left(i_{o,q}^{ref} - i_{o,q} \right) + K_I^I . x_{i,q} \\ +L_f . \omega^{ref} . i_{o,d} + K_{ffv} . v_{pcc,q} \end{bmatrix} \tag{26}$$

$$\begin{bmatrix} \frac{dx_{i,d}}{dt} \\ \frac{dx_{i,q}}{dt} \end{bmatrix} = \begin{bmatrix} i_{o,d}^{ref} - i_{o,d} \\ i_{o,q}^{ref} - i_{o,q} \end{bmatrix} \tag{27}$$

The modulation index (m_{abc}), which is used to get the PWM signal, is obtained by (28).

$$m_{abc} = \frac{2 v_{abc}^{ref}}{v_{dc}^{ref}} \tag{28}$$

DC current reference is obtained by (29). K_{dc} value is calculated as in (30). Switching and DC losses are also considered.

$$i_{dc}^{ref} = K_{dc} \left(v_{dc}^{ref} - v_{dc} \right) + \frac{P^{ref}}{v_{dc}^{ref}} + \left(\frac{v_{dc}}{R_{dc}} + \frac{v_{dc} i_x - P}{v_{dc}^{ref}} \right) \tag{29}$$

$$K_{dc} = \frac{100 S_b}{\left(v_{dc}^{ref} \right)^2} \tag{30}$$

B. SYSTEM LEVEL CONTROL

The GFM and GFL control methods discussed in previous sections are applied at the system-level. The system-level control blocks and inputs and outputs of the system are given in the middle of Fig. 14. The voltage reference (v_{pcc}^{ref}) is provided by the system-level control in GFM converters, while the current reference is provided in GFL converters for inner controllers.

The system-level control consists of APC and RPC blocks. APC and RPC do not affect each other if a converter is connected to the grid with inductive lines. Namely, while active power is controlled based on frequency, reactive power is controlled based on voltage. When the inductive character of the line decreases, APC and RPC control loops interact with each other.

The literature introduced two methods to address the interaction between APC and RPC. The first method is to increase the equivalent impedance by adding a virtual impedance. This reduces the interaction between the P-f and Q-v loops. The second method is to use a Multi Input Multi Output (MIMO) control structure. In this case, the P-f and Q-v loops do not need to be decoupled. This method is effective for inductive and non-inductive line characteristics [82]. Some studies were conducted on estimating the grid impedance and determining the adaptive impedance accordingly [47], [83]. The prediction algorithms that were used to estimate the grid impedance of grid-connected converters are as follows [47]: extended Kalman filter [84], recursive least square [85], system identification [86], power variations [87], single frequency injection techniques [88], orthogonal binary sequence [89], pulse injection [90], [91].

C. GRID SYNCHRONIZATION

The synchronization unit plays a crucial role in ensuring the stable operation of grid-connected converters. There are two fundamental synchronization techniques: PLL and PSC. While GFL converters use PLL, GFM converters generally use PSC for synchronization. Among these, PLL is disadvantaged in weak grids, whereas PSC is disadvantaged in strong grids.

IEEE standard 1204-1197 defines the strength of an AC/DC system according to SCR. When short-circuit ratio (SCR) is greater than 3, the system is called ''strong''. If the SCR value is between 2 and 3, the system is referred to as ''weak''. An AC/DC system with an SCR value less than 2 is called ''very weak'' [92].

In GFL converters, as the SCR decreases (in weak grids), it leads to a small-signal stability problem caused by the PLL since they interact with each other [93]. The most commonly used PLL type is the ''type 2 SRF PLL'' described in [94]. This method achieves synchronization by reducing the q component of voltage using a PI controller, thus aligning the $d-axis$ of the SRF with the output voltage vector [40], [95], [96], [97]. In equation (31), K_P^s and K_I^s are the proportional and integral control gains of the synchronization unit, where ω_0 represents the 1 per unit (p.u.) nominal angular frequency, and ε represents the integral term of the q-axis voltage.

$$\dot{\varepsilon} = v_{pcc}^q \tag{31a}$$

$$\omega_s = \omega_0 + K_P^s v_{pcc}^q + K_I^s \varepsilon \tag{31b}$$

$$\dot{\theta}_s = \omega_b \omega_s \tag{31c}$$

GFM converters perform better in weak grids due to their voltage source nature and the ability to self-synchronize with the help of PSC [6], [98], [99]. PSC-based power synchronization is achieved with three methods in GFM converters [70]. The first method is based on synchronization through power imbalance applied in droop and VSG control. The second method relies on the current flow, which is applied in VOC-based control. The third method is based on DC voltage and DC energy imbalance and is used for synchronization in matching control.

Recently, to address the shortcomings of PLL and PSC, a hybrid synchronization control (HSC) was proposed and the impedance characteristics of HSC and PSC were compared in [100]. Two types of HSC were suggested: Type 1-based HSC and Type 2-based HSC. The impedance of Type 2-based HSC has a smaller magnitude compared to PSC and achieves a better phase margin at the fundamental frequency. On the other hand, the impedance magnitude of Type 1-based HSC is higher compared to PSC, resulting in a worse phase margin.

The concept of ''complex frequency synchronization'' was proposed in [75] to study the phase angle-voltage

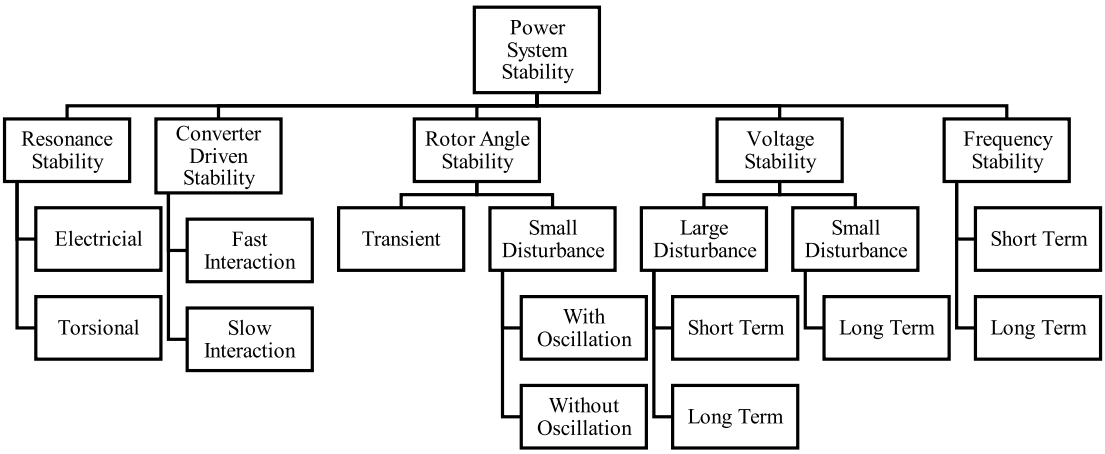

FIGURE 15. Power system stability [101], [102], [103].

magnitude stability of a power converter controlled by VOC. For this purpose, the system was formulated as linear fast and slow systems. The linearity property of the system makes it easier to analyze fast complex frequency synchronization and slower voltage stabilization. Complex frequency synchronization also includes synchronization of the rate of change of voltage (RoCoV) in addition to angle and frequency.

D. SYSTEM STABILITY

Stability in power systems is traditionally ensured by SGs, and it is addressed in terms of rotor angle, voltage, and frequency. However, with the increasing prevalence of IBRs, new topics such as converter-driven stability and electrical resonance stability are added to the subject. The stability of the power system, taking into account these new conditions, is classified in Fig. 15.

Converter-driven stability occurs in the form of oscillations and is entirely related to the control of IBRs. Fast and slow interaction scenarios are being examined separately in [102]. Fast interaction refers to the situation where the control systems of IBRs exhibit fast dynamic interaction with other fast-responding elements of the power system and other fast power electronic equipments. Slow interaction, on the other hand, occurs when the control systems of IBRs exhibit slow dynamic interaction with other slow-responding elements of the power system.

Resonance stability comes in two forms: torsional and electrical resonance stability [102]. Torsional resonance stability occurs in traditional grids, in SGs. However, high voltage direct current (HVDC) and flexible alternating current transmission systems (FACTS) as power electronics-based systems affect this type of stability. Electrical resonance stability occurs in a grid involving renewable energy sources, especially in variable-speed asynchronous generators such as double-fed induction generators (DFIG). It exhibits the following effects [103]: causes oscillations in current and voltage, leads to significant disturbances in electrical torque, and adversely affects electrical and mechanical components. Other forms of stability in traditional power systems are discussed in detail in [104].

Many studies have been conducted in the literature to evaluate the stability of power systems with GFM converters. In [105], stability analysis of GFL and GFM converters was obtained based on state space modeling leveraging eigenvalue trajectories. The synchronization and frequency stability of VSG during faults were improved by adding a transient damping method in the active power control loop in [106]. Small signal stability analyses of single loop and double loop droop control were done in [72]. The effects of transmission line dynamics on dVOC-based converters were analyzed in [107]. In [99], the robust stability of parallel connected synchronverters was investigated based on μ-analysis using structured singular values and it was demonstrated that parallel operation reduced robust stability. Also, virtual impedance was proposed as a solution.

E. FAULT RIDE THROUGH

Ride through or FRT is the capability to endure voltage or frequency disturbances within specified limits and maintain proper operation [78]. Voltage disturbance ride-through, and frequency disturbance ride-through requirements for IBR plants are given in IEEE 1547-2018 [78] and IEEE 2800-2022 [79] standards. Applicable voltage and frequency levels, operating modes, and minimum ride-through times are detailed in the standard.

Faults can lead to synchronization problems in GFM converters, which can cause severe instabilities, low-frequency oscillations, and distortions in the current signal [108]. Effective FRT requires (i) synchronization with arbitrarily low grid voltage and (ii) fast overcurrent limiting capabilities [69]. Numerous studies recommend switching to GFL mode in the event of a fault in the GFM converter. However, as the proportion of SGs decreases significantly in a power system, converters need to maintain their voltage mode characteristics and be resilient to weak grid conditions [109].

In [108], a new VSG-based GFM control strategy was proposed to maintain the GFM feature while simultaneously improving performance in case of faults. The suggested controller synchronized the GFM converter by altering the virtual inertia and performing positive-sequence virtual impedance calculations, even in unbalanced and severe fault conditions. A fault mode controller was proposed in [109]. The controller limited the fault current to an acceptable level while ensuring that the converter remained in voltage mode. The uVOC strategy proposed in [69], provides effective FRT capability for symmetrical faults. The dsUVOC strategy proposed in [76] offers asymmetric FRT without the need for a redundant controller and PLL. It can synchronize both positive and negative sequences simultaneously. The classical current-limiting strategies can cause transient instability and loss of synchronization. To this end, a new method called ''cross-forming control'' is proposed to limit fault currents for GFM converters, in [110].

F. SYSTEM PROTECTION

An SG is capable of withstanding overcurrents up to five times its nominal current [111]. However, power electronic components within converter-interfaced generation units have lower overcurrent tolerance [112]. A VSC can withstand fault currents up to 50-60% above its nominal current value [113].

Current limiting is more challenging in a VSC compared to current source converter (CSC). Since a GFL converter is controlled as a current source and provides a current reference to the device-level controller, it can easily limit overcurrent in both balanced and unbalanced grid conditions [114]. In the GFM structure, the current is calculated at the device level based on the controlled voltage at the PCC. This can lead to instantaneous spikes in current during any disturbance while the converter attempts to regulate voltage and frequency [70]. So current limiting is highly crucial in GFM converters. The structure of GFM converters, the voltage sources behind the impedance, make them robust against changes in SCR but more vulnerable to significant disturbances. Therefore, GFM converters need to have control algorithms to (i) ensure stable operation under various grid conditions, (ii) handle overloads caused by faults, and (iii) re-synchronize reliably after the fault is cleared [115].

Two different current limiting strategies were proposed in the literature [109], [116], [117], [118], [119], [120], [121], [122], [123]: (i) current limiting through the virtual impedance method [124] and (ii) current limiting via the reference current saturation method [122], [125]. An extended power synchronization method was proposed in [115], which allows the system to operate under both balanced and unbalanced grid conditions while meeting the FRT requirements. The study in [126] included a current reference limiting strategy related to the transient stability of GFM converters. The impact of the current reference angle on transient stability was investigated. Analytical formulas were derived to predict the critical clearing angle (CCA) and the critical clearing time (CCT) by considering different current reference angle values, for a balanced voltage sag scenario. In [57], an optimal protection coordination (OPC) program with FRT capability in accordance with grid codes was developed for synchronverters in a microgrid. Therefore operating times of time-current-voltage overcurrent relays (TIV-OCRs) were minimized. In [127], a virtual impedance fault current limiter with a synchronverter was used in the OPC scheme, maintaining voltage source characteristics during faults and enhancing transient stability.

G. BLACK START

Power system restoration, vital to operation and planning, involves returning generators and restoring power after major outages, such as a blackout [128]. The converter-based sources need to have black start capability for effective participation in system restoration after a blackout [129]. Not all GFM IBRs can provide black-start services, as this may need extra hardware, design, and functions, leading to higher costs and requiring special coordination with system operators [130]. When determining whether a resource has black start capability, the following criteria are taken into consideration: station power requirement, startup time, ramp rate, active and reactive power capacity, on-site fuel/energy supply, operation during frequency excursions, stabilizing system frequency and location [131].

Using PV and wind generation units in black start is very difficult because of their uncertain nature, but BESS units are possible for this purpose [131]. However, updated grid codes are imperative to integrate renewable power plants such as wind and photovoltaic (PV) in the system restoration process. These plants need to be able to control frequency and voltage in an isolated grid to restart the system [132].

While GFL converters lack a black start capability due to their dependency on the grid voltage signal, GFM ones may inherently have this capability. Moreover, research can be conducted to provide a black start capability for GFL converters by providing an external voltage reference. Equipping converter-based systems with a reliable black start capability is one of the current research areas in the literature [21], [132], [133], [134], [135].

In the system energization process, first the transformers and cables in a network are energized. Energizing the transformer, without any control, can cause inrush currents reaching up to 6-10 times the rated capacity [135], [136]. In reference [135], the voltage and power loops of the VSG control were modified to be softly energized to reduce transformer inrush current in black start applications.

In June 2021, on-site black start tests and EMT simulation studies were conducted within the scope of the RINGO project for 12 MW/ 24 MWh GFM-controlled BESS connected with a 10 MW GFL-controlled Wind Farm and some loads, which are located in a small part of a bulk power system, in Vingeanne, France [137]. It is

underlined that this is the first worldwide successful black start test of a system including GFM BESS and GFL Wind Farm. The circuit diagram of tested system is given in Fig. 16. System restoration was performed in three steps in both on-site and EMT simulations. In the Test 1A phase, a 17 MVA transformer, 200 m underground cable, and 36 MVA transformer were softly energized sequentially by GFM BESS. Then, 14.6 km cable was energized in the Test 1B stage. In the Test 2 phase, first the auxiliary load of the wind farm was supplied, and then the 10 MW Wind Power Plant was connected to the system. This isolated network was connected to the transmission network at 63 kV level in the Test 3 phase. After an hour, BESS seamlessly transitioned from GFM mode to GFL mode. Also, the effect of the initial flux of transformers on inrush current was studied.

H. SEAMLESS TRANSITION BETWEEN GFL AND GFM MODES

In an electrical grid that includes asynchronous renewable energy sources, the instantaneous SG rate and system inertia constantly change as these sources are intermittent in nature. In terms of stability, it is more appropriate for the converter to operate in GFL mode when the SG ratio is high and in GFM mode when it is low. Therefore, the ability to operate in both GFL and GFM modes and to transition smoothly between them is an advantage for a grid connected converter.

The idea of a converter operating in both GFL and GFM modes has attracted the interest of many researchers in the literature. An optimized controller based on a multi-dimensional Pareto Front algorithm was proposed in [138]. Depending on the sensitivity function and weighting function, the converter can operate in both GFL and GFM modes. Reference [139] proposed an H_∞-based control method to design a droop controller that can operate in both GFM and GFL modes. The values of the sensitivity and weighting functions were tailored to the control objectives. In [140], a control method was presented for IBRs to operate in GFL and GFM modes. The proposed controller utilized two different parallel control paths. Both control paths provided the phase angle and magnitude of the PWM reference signal. Depending on the operating mode of the inverter, the pulse-width modulation (PWM) generator received the reference signal from only the relevant path at a time. The proposed controller could keep the two control paths in sync, allowing inverters operating in GFL mode to smoothly transition to GFM mode and created a microgrid simultaneously when they suddenly disconnect from the grid.

I. SEAMLESS TRANSITION BETWEEN ISOLATED AND GRID-CONNECTED MODES

One of the key features of a GFM converter is its ability to switch between isolated and grid-connected modes. However, the transition can introduce significant voltage, current, and frequency fluctuations [141]. Several studies have been conducted to mitigate the adverse effects of this issue. In [142], a hierarchical control structure for VOC-controlled converters is proposed for seamless transitions between isolated and grid-connected modes in a microgrid. In [141], an adaptive model predictive control (AMPC) method was developed for GFM converters to achieve a smooth transition from islanded mode to grid-connected mode and balance the trade-off between frequency stability and response speed. In [69], the uVOC method was enabled to operate in both grid-connected and isolated modes, with seamless transition between these two modes.

IV. GFM PRODUCTS, COMPLETED AND ONGOING PILOT PROJECTS

Although GFM applications are not prevalent worldwide, there are some completed and ongoing GFM projects implemented by energy companies, research centers, transmission system operators (TSOs), and component manufacturing companies. The voltage levels of applications are LV, MV, and HV, with a diverse range of rated power and energy capacities. The projects include some GFM and grid support functionalities such as ancillary services, energy management, black start, islanded operations, and renewable integration.

GFM pilot projects completed by 2021 are summarized in [16]. This study expands on these by adding recently completed and ongoing projects. Completed projects are categorized by system type, including BESS installations, GFM wind turbine projects, hybrid sources, and HVDC applications. All projects completed between 2012 and 2023 are given in Table 3. The second section includes ongoing and planned projects.

A. GFM COMPANY PRODUCTS ON THE MARKET

Some GFM products for BESS, hybrid power plant, HVDC, and Static Synchronous Compensator (STATCOM) applications have started to appear on the market. PCS100 ESS inverter of ABB, e-mesh PowerStore of Hitachi Energy, Proteus PCS-E inverter of Siemens, and LUNA2000-200KTL-H1 Smart PCS of Huawei are used for GFM BESS applications. The Sunny Central Storage inverter of SMA is used for hybrid applications. Modular Advanced Control for HVDC (MACH) equipment of Hitachi Energy is used for HDVC and STATCOM applications.

PCS100 ESS with ratings from 100 kVA to 4000 kVA is a GFM inverter of ABB that uses virtual machine emulation-based control technology that provides voltage stability, frequency regulation and dynamic system response. It allows both active and reactive power control and provides a seamless transition between grid-connected and islanded modes. It has features such as low-voltage ride-through capability and black start functionality. It has been installed in system-level projects with a rated power exceeding 30 MVA through parallel connection [143]. Hitachi acquired 80.1% of ABB's Power Grids business in 2020, subsequently renaming it Hitachi Energy [144]. Hitachi Energy's product with GFM feature is the "e-mesh PowerStore", which has power

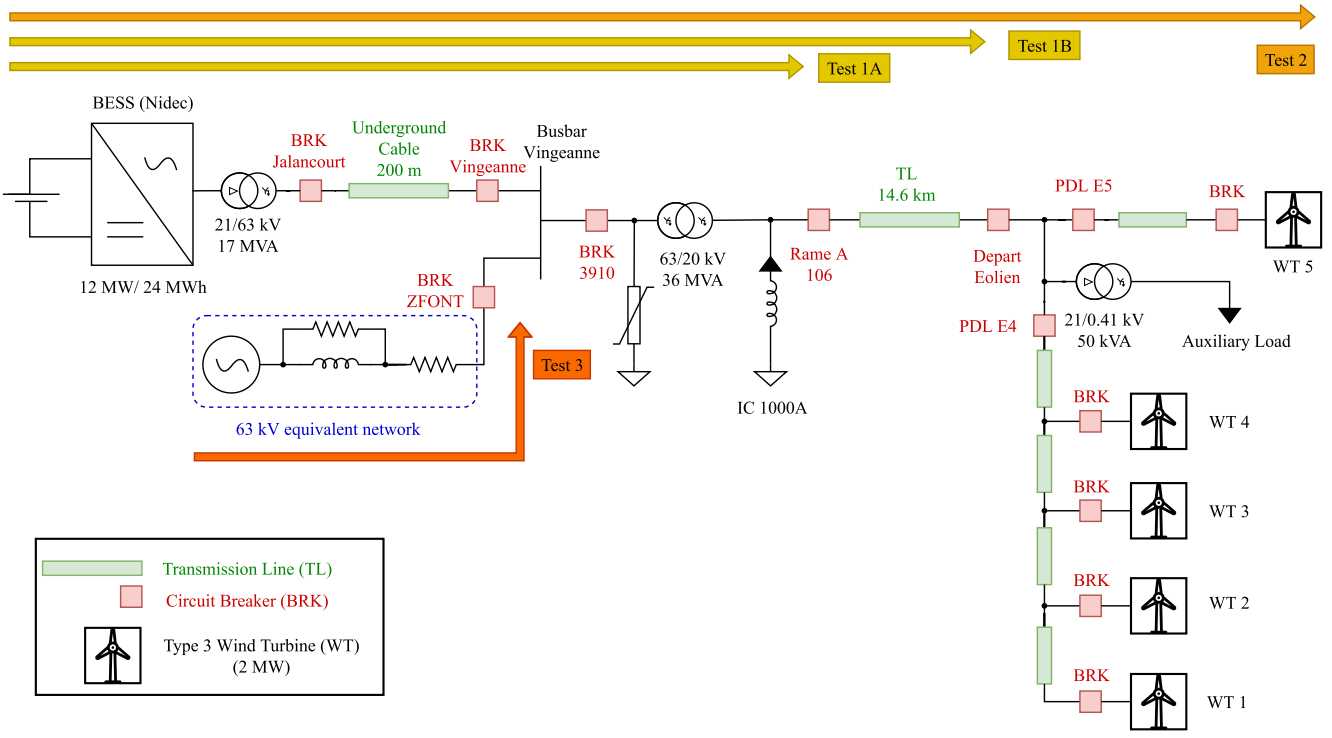

FIGURE 16. Circuit diagram and system restoration steps of the RINGO black start project [137].

ratings from 250 kW to MW scale. The system operates in both grid-connected and isolated modes, employing virtual generator mode algorithms to deliver inertia and fast voltage and frequency support. It includes current limiting during faults and inrush, supports centralized and decentralized methods, and features black start capability [145]. Siemens Gamesa released a 1500 V "Proteus PCS-E" battery inverter that could be operated in both GFL and GFM modes in 2023. It could provide fast frequency response and synthetic inertia. It has four quadrant operation for full active and reactive power support. It has black start capability and 5 different nominal AC Power options ranging from 4446 kVA to 5477 kVA [146].The Huawei LUNA2000-200KTL-H1 Smart PCS is a 200 kW device capable of grid forming and black start operations [147].

"Sunny Central Storage 1900 / 2200 / 2475 / 2900" products are SMA's GFM inverters delivering maximum AC power of up to 2900 kVA, provide ancillary grid services, allow setpoints for active and reactive power, and offer both static grid support (Q(U), P(f)) and dynamic grid support (FRT). They offer ramp-rate control of PV power and black start functionality. They can be for hybrid systems including sources such as BESS, PV, and diesel generators [148].

Hitachi Energy provides a GFM-enabled control system called "Modular Advanced Control for HVDC (MACH)" to control VSC-HVDC systems. MACH equipment can also be used for Flexible Alternating Current Transmission System (FACTS) devices such as STATCOM by differentiating its software [149]. "SVC Light Enhanced" is a GFM-enabled STATCOM device with supercapacitors as storage units, providing both active and reactive power, dynamic voltage regulation capability, inertia response, and fault current contribution [150]. "SVC PLUS FS" is Siemens Energy's STATCOM, which provides dynamic voltage and frequency support and high active power to the grid by simulating system inertia when necessary [151].

B. COMPLETED GFM PROJECTS

1) BESS INSTALLATIONS

One of the first GFM applications is the Zurich Battery Energy Storage (BESS) Project with 1 MW rated power. The project was initialized in 2012 for primary frequency control, peak shaving, and islanded operations. The system was operated in both VSC and CSC modes [16], [152]. ABB's PCS 100 converter was used for the project [153]. The Hornsdale Power Reserve project, which was installed in South Australia in 2017 and expanded in 2020, is a VSG-based GFM-BESS project, with a 150 MW/194 MWh capacity. The BESS has provided fast frequency response and synthetic inertia services [16]. The General Electric (GE) company has been studying GFM projects and developing GFM technologies. The company first installed a lithium-ion BESS connected via 30 GFM-controlled inverters in 2017 in order to support the grid [16]. The Dalrymple BESS (ESCRI-SA) project, VSG-based 30 MVA/8 MWh GFM BESS, was completed on the Lower Yorke Peninsula of Australia in 2018. The DEMOCRAT (DEMOnstrator of a miCrogrid

TABLE 3. Completed GFM projects (adapted from [16]).

Project Name	Location	Year	Rated Power and Enegy Capacity	System Type
Zurich BESS	Switzerland	2012	1 MW / 0.58 MWh	BESS
Hornsdale Power Reserve	Australia	2017 - 2020	150 MW / 194 MWh	BESS
Dalrymple BESS (ESCRI-SA)	Australia	2018 - 2019	30 MW / 8 MWh	BESS
DEMOCRAT Project	Europe	2018	0.2 MW / 0.109 MWh	BESS
Bordesholm BESS	Germany	2019	15 MW	BESS
Torrens Island BESS	Australia	2023	250 MW/250 MWh	BESS
Dersalloch Wind Farm	Scotland	2019	69 MW	GFM Wind
Mackinac HVDC	USA	2012	200 MW	HVDC
Ausnet GESS	Australia	2012	1 MW / 1MWh BESS + 1 MW diesel generator	Hybrid (BESS + Diesel generator)
OSMOSE Project	Europe	2018 - 2022	0.1 – 0.72 MW / 0.025 - 0.56 MWh	Hybrid (BESS + Supercapacitor)
St. Eustatius II Project	Netherlands	2017	4.15 MW PV + 5.9 MWh BESS + 4 MVA diesel generator	Hybrid (PV + BESS + Diesel generator)
Tetiaroa Island	French Polynesia	2018	1.2 MVA diesel generator + 1.3 MWp PV plant + 2.6 MWh BESS	Hybrid (PV + BESS + Diesel generator)
Saba Island	Netherlands	2019	4 MVA diesel generator + 2 MWp PV plant + 2.3 MWh BESS	Hybrid (PV + BESS + Diesel generator)
Graciosa Island, Canary Islands	Spain	2018	1 MW PV + 4.5 MW of wind + 6 MW / 3.2 MWh BESS	Hybrid (PV + Wind + BESS)
La Plana Hybrid Project	Spain	2018	850 kW wind + 245 kW PV + 3x222 kW diesel generators + 3x 435 kW/145 kWh + 120 kW/400 kWh BESS	Hybrid (Wind + PV + diesel generators + lithium-ion BESS + redox-flow BESS)
NREL's Wind Turbine at Flatiron Campus	USA	2019	8 MW wind + 1.5 MW PV + 1.25 MW/1.25 MWh + 1 MW/1 MWh BESS	Hybrid (Wind + PV +BESS)

integRAting sTorage) project, owned by Efacec was installed in 2018 in Portugal. The project involved GFM-controlled storage devices that could operate in an LV distribution grid or standalone mode to keep voltage and frequency within limits and black start. The system included two lithium-ion batteries with a capacity of 200 KW/109 KWh and a 250 KVA GFM-controlled inverter [16], [154]. The VSG-based GFM technology that provides synthetic inertia, high fault current, and flexibility services such as fast power injection, seamless islanding, and black start was implemented in the project [16], [155]. RES Deutschland GmbH installed the BESS, which has a capacity of 15 MWh, to provide frequency control services in Bordesholm, Germany, in 2019. The plant can serve a 10 MW primary reserve for frequency control [156], [157]. In South Australia, the grid-scale Torrens Island BESS Project with 250 MW/250 MWh capacity was completed by Wärtsilä on behalf of AGL Energy in 2023 and used SMA's inverters. The system can operate in GFL and GFM modes via VSG control [158].

2) GFM WIND TURBINE PROJECTS

69 MW wind farm including 23 turbines of Siemens-Gamesa, in Dersalloch (Scotland) owned by Scottish Power Renewables was operated in GFM mode with VSG control for approximately 6 weeks, from May to June of 2019 [16], [159]. 2.5 MW Type III wind turbine was operated in GFM mode at NREL's Flatiron Campus. The subsynchronous resonance between wind power plants was investigated [160].

3) HYBRID PROJECTS

AusNet Grid Energy Storage System (GESS) was started in 2012 in Melbourne, Australia. It was constructed by the consortium led by ABB on behalf of AusNet Services, an energy delivery company. The AusNet GESS project includes a 1 MW backup diesel generator, a 1 MW/1 MWh battery, and a GFM inverter that is used to support the grid with the capabilities of peak shaving, power factor correction, voltage support, phase load balance, and islanded operations [16], [161]. SMA has led numerous large-scale hybrid GFM projects around the world. St. Eustatius II Project was launched on St. Eustatius Island in 2017 to reduce the rate of diesel generators by installing hybrid PV and BESS sources with GFM features. The system has a capacity of 4.15 MW PV, 5.9 MWh BESS, and 4 MVA diesel generator. SMA commissioned another project on Tetiaroa Island, French Polynesia, in 2018. The system consists of a 1.2 MVA diesel generator, 1.3 MWp PV plant, 2.6 MWh BESS with black start capability. The diesel generator with the capacity of 4 MVA was supported by a 2 MWp PV plant and 2.3 MWh batteries on Saba Island with GFM features in 2019 [16]. Wärtsila implemented a hybrid power system on Graciosa Island to integrate 1 MW of PV, 4.5 MW of wind power, and a 6 MW/3.2 MWh energy storage system through SMA's converters with GFM and black start capability in 2018 [162]. In addition to its flexible operation feature that allows parallel use with various power sources, it demonstrated an effective control interface that facilitates synchronization and black start capability [156]. La Plana Hybrid Power Plant Project of Siemens Gamesa was installed in 2015. The plant includes an 850 kW wind turbine, a 245 kW PV system, 3 $\times$ 222 kW diesel generators, 3 $\times$ 435 kW/145 kWh lithium-ion BESS and 120 kW/400 kWh redox-flow BESS units. Storage units provide ancillary services, such as frequency reserve and regulation, peak shaving, synthetic inertia, and black start, thanks to their GFM capability [16]. A hybrid power plant consisting of an 8 MW wind farm, 1.5 MW PV plant, and droop-controlled two BESS with 1.25 MW/1.25 MWh

and 1 MW/1 MWh capacities was installed on the National Renewable Energy Laboratory (NREL) Flatirons campus, in Colorado, USA, in 2019. The GFM-controlled storage devices were used for ancillary services and renewable integration [16], [163]. 7.4 MW BESS was used to achieve the black start of a 150 MW gas turbine at Perryville Power Station in 2019 [16], [164]. The OSMOSE Project, supported by the European Union's Horizon 2020 program, was carried out by 33 partners between 2018-2022. Three grid-forming demonstrators were investigated in the project. The first one included a utility-scale 720 kW/560 kWh lithium-titanate-oxide-based battery and 720 kVA converter that could be operated in both GFL and GFM modes at Ecole Polytechnique Fédérale de Lausanne (EPFL), Switzerland. The second demonstrator at the EPFL campus was composed of a small-scale 25 kWh LTO battery and a 25 kW 4-quadrant converter that operated in both GFL and GFM modes. The third one is a hybrid energy storage system that includes a 0.5 MVA lithium-ion battery and 1 MVA supercapacitor rack with 1 MVA GFM inverter [16], [165].

4) HVDC PROJECT

Mackinac back-to-back, VSC-HVDC project, which has 200 MW and 100 MVAR bidirectional power transfer capacity, was started in 2012 by the American Transmission Company to manage power flow between the Upper and Lower Peninsulas of Michigan, necessitating operation under weak grid conditions while addressing prevalent issues like voltage oscillations and faults. The VSC-HVDC exhibited features including autonomous control over both active and reactive power, black start capability, and functioning in STATCOM mode [16], [166].

C. ONGOING AND PLANNED PROJECTS

There are ongoing and about to start GFM projects around the world. The construction of the Broken Hill BESS project, owned by AGL in Australia, started in 2022 and will be commissioned in 2025. The project consists of lithium-ion batteries with 50 MW/50MWh capacity and was aimed to improve grid strength and enhance stability with GFM futures [167], [168]. The Liddell Battery Project, with a capacity of 500 MW/1000 MWh, is going to be installed by AGL between 2024 and 2026 in New South Wales, Australia [169]. The lithium-ion-based GFM-controlled 100 MW/200 MWh Palmerston BESS project was proposed by Akaysha Energy in Tasmania, Australia. VSG technology will be used to provide system strength and inertia services in the project [170]. Another large-scale GFM BESS project is Statkraft's Neilston Greener Grid Park Project with an installed capacity of 50 MW in Scotland, the construction of which started in 2023 and is planned to be completed in 2024 [171]. Statkraft's other GFM BESS project in Scotland is the Coylton Greener Grid Park Project, with a capacity of 50 MW. The main planning application was made in 2023 and installation will be completed within 12–18 months after commencement [172]. Zenobe will implement three GFM-controlled BESS projects at Blackhillock, Kilmarnock, and Eccles in Scotland by 2026 [174]. The Blackhillock BESS Project was launched in Scotland in 2023. The project has two stages. Phase 1 with 200 MW/400 MW capacity will come into operation in the summer of 2024, and Phase 2 with a 100 MW/200 MWh capacity will come into operation in 2026. To improve the reliability of the renewable-rich power system in the UK, the site will provide stability services to the National Grid ESO [173]. The second one is the 300 MW/600 MWh Kilmarnock South BESS Project, which will provide short-circuit level and inertia. Its location was selected to reduce the curtailment of wind farms. Phase 1 (200 MW / 400 MWh) will be commissioned in 2024. Zenobe's third project is the 400 MW/800 MWh Eccles BESS Project, which will be put into operation in 2026 [174].

The ongoing and planned BESS projects detailed above are given in Table 4.

TABLE 4. Ongoing and planned projects.

Project Name	Location	Ending Year	Rated Power and Enegy Capacity	System Type
Neilston Greener Grid Park Project	Scotland	2024	50 MW	BESS
Coylton Greener Grid Park Project	Scotland	2024	50 MW	BESS
Blackhillock BESS - Phase 1	Scotland	2024	200 MW/400 MW	BESS
Kilmarnock BESS - Phase 1	Scotland	2024	200 MW / 400 MWh	BESS
Broken Hill BESS	Australia	2025	50 MW / 50MWh	BESS
Liddell Battery Project	Australia	2026	500 MW/1000 MWh	BESS
Blackhillock BESS - Phase 2	Scotland	2026	100 MW/200 MWh	BESS
Kilmarnock BESS - Phase 2	Scotland	2026	100 MW / 200 MWh	BESS
Eccles BESS	Scotland	2026	400 MW/800 MWh	BESS
Palmerston BESS	Australia	-	100 MW/200 MWh	BESS

V. RESEARCH DIRECTIONS FOR ADVANCED GFM CONTROL APPROACHES

Due to the decreasing SG ratio,it is expected that IBRs not only provide power to the grid but also possess features such as enhancing and supporting the dynamic performance of the grid, operating in grid-connected and isolated modes, and black start capability. As the need for system requirements to be met by IBRs increases, research has led to the development of advanced control approaches that enhance the performance of GFM converters. For this purpose, hybrid control approaches including multiple GFM features, advanced controllers enabled by MIMO system models, coordinated control of converters, and control design based on new modeling approaches such as complex frequency have become substantial and essential. Studies related to advanced control approaches in the literature were examined under the four main headings shown in Fig. 17. These research topics are quite new and there are many opportunities for improvement and development in these areas.

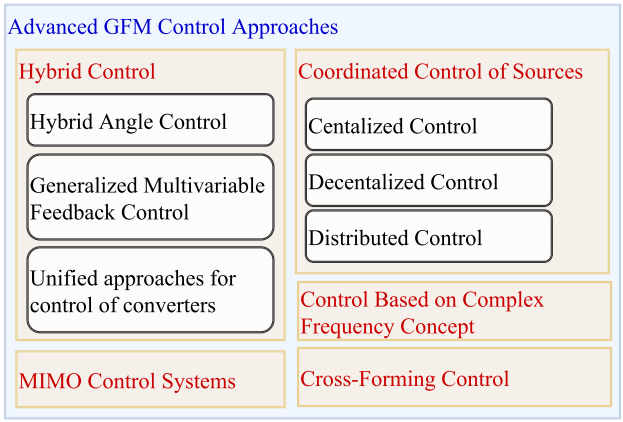

FIGURE 17. Advanced GFM control approaches.

A. HYBRID CONTROL

1) HYBRID ANGLE CONTROL

In the literature, there are studies that achieve superior performance by combining multiple control methods. Control methods such as droop control, VSG, and dVOC, where the converter is controlled based on AC-side measurements, enhance small-signal frequency stability. DC measurement-based methods, such as matching control, are more robust to operating conditions as the device current approaches its limits. A new hybrid angle control (HAC) method was proposed in [75], where AC-based droop control and DC-based matching control were combined to determine the converter's frequency. The hybrid use of other control methods in this field will provide new valuable results.

2) GENERALIZED MULTIVARIABLE FEEDBACK CONTROL

Different control methods exhibit distinct advantages over each other, as explained in Section II-C. Combining these methods and bringing their superior features together is the focus of interest of researchers. In the literature, this has been achieved by performing feedback control in a multivariate system consisting of mathematical equations of different controllers. Reference [49] combined some control strategies such as droop, PSC, VSG, dVOC, matching, and their derived versions in the ''multivariable feedback control transfer matrix''. A generalized GFM converter architecture was proposed using multivariable feedback control theory. In [175], the MIMO-GFM converter control approach was proposed, which used multivariable feedback control, focused on the direct control of frequency and internal voltage as state variables, and effectively reduced the effect of high-frequency components. Chen et al. [176] introduced a MIMO-GFM control system for power converters, employing a multivariable feedback structure that couples AC and DC loops through a general multivariable control transfer matrix. This approach promises a wide field of study for researchers, as it allows the application of various modern control methods as power systems become increasingly complex.

3) UNIFIED APPROACHES FOR CONTROL OF CONVERTERS

Unified control of power converters allows them to operate in different modes using a single model and synthesize different methods. VSG-based IBRs operate differently in grid-connected, islanded-single-generator, and islanded-multi-generator modes. A unified modeling method was proposed to analyze their dynamic performances in each mode in [177]. Unlike VSG, Droop control has better power reference tracking capability and a high RoCoF in islanded mode due to the lack of inertia. However, VSG tends to cause significant deviations and longer settling times in grid-connected mode. A second-order generalized droop controller (GDC) based on both droop and VSG control was proposed in [178] to better operate in both operation modes. In [179], a unified voltage control scheme, which is composed of three loops, i.e., (i) the voltage magnitude control, (ii) the virtual impedance control, and (iii) the voltage-reference-feedforward control, was proposed for grid-forming inverters that enable to synthesize six commonly used voltage control methods, i.e. (i) PI-based dual-loop vector-voltage control (VVC), (ii) virtual admittance control (VAC), (iii) VAC with the PCC voltage magnitude regulation, (iv) single-loop voltage-magnitude (SLVM) control, (v) SLVM control with the virtual resistance and (vi) active resistance control.

B. MULTI INPUT MULTI OUTPUT (MIMO) CONTROL SYSTEM DESIGN

A typical GFM converter includes multiple cascaded control loops, such as inner voltage and current loops, as well as outer active and reactive power loops. The bandwidth of the inner-cascade control loops is chosen wider than the outer power control loops to facilitate analysis and design and prevent interaction of control blocks. This allows separate examination of the fast dynamics of inner loops and the slow dynamics of outer loops [6]. However, multiple loops have complex dynamics over a wide frequency range. Therefore, some challenges arise in operation, analysis, and control in low-inertia systems [85].

Single input single output (SISO) control structures and classical design methods frequently used in control of GFM converters have limitations in (i) low-inductive line applications and (ii) achieving the desired/appropriate performance [82]. Controlling P and Q separately becomes harder as the R/X ratio of the transmission line and the power angle between the GFM converter and grid voltages increase, due to interaction between the P and Q control loops [83]. When cascade SISO controllers interact, MIMO controller designs become significant. MIMO control structures have distinct advantages, especially in the following situations: (i) when the R/X ratio of the line and the power angle are large [83], [87], (ii) when the features of multiple GFM control methods are desired to be used together [87], and (iii) when strict tracking of performance criteria from the converter is required [49], [86]. The disadvantage of MIMO control is its need for a high-degree controller and

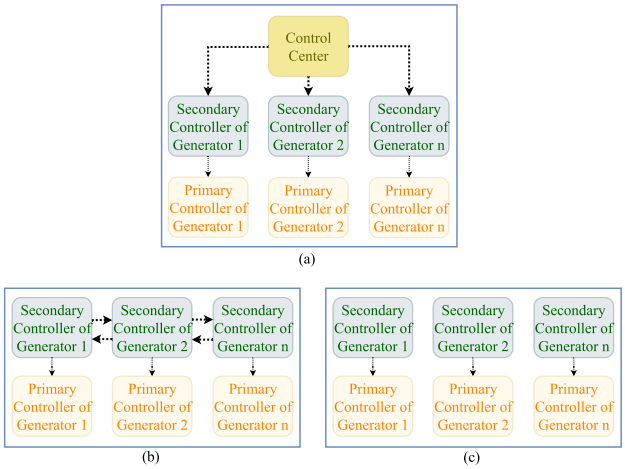

FIGURE 18. Secondary control of a microgrid: (a) centralized, (b) distributed, (c) decentralized [94].

high-capacity processor, making implementation costly. This can be mitigated with model reduction techniques [88].

C. COORDINATED CONTROL OF SOURCES

The coordinated control of resources to meet system requirements is highly important in microgrids and virtual power plants (VPPs). Three different control frames are used for coordinated control: centralized, decentralized, and distributed control. In the first method, setpoints are determined by the central control unit, and there is a communication network between the central control unit and the controlled components [90], [91]. The second is decentralized control [93], [94], which involves peer-to-peer communication and control processes.

There are many studies in the literature about coordinated control in microgrids. The demand was distributed among various PV inverters using a decentralized method in [95]. The third is distributed control [96], [97] during blackstart. This method does not require a communication network since each device is controlled according to grid measurements at the node it is connected to. In a microgrid, three control schemes were applied as secondary control as shown in Fig. 18 to add correction terms, and to mitigate steady-state errors in voltage and frequency [94].

In a VPP, distributed generators are aggregated to act as a single power plant. They can provide voltage and frequency support to the system [180]. The parameter values required for control loops are adjusted based on the stable operation of a single converter; however, system behavior is also taken into account in VPPs. The utilization of power sources within VPPs for ancillary services was initially proposed in [181]. Dynamic VPP goes beyond tracking reference setpoints in a system accommodating different types of sources and dynamically provides the desired ancillary services [182]. The dynamic VPP proposed in [182] offers dynamic ancillary services on faster time scales, such as fast frequency and voltage control. The study used a heterogeneous set of sources with complementary features such as energy/power availability, response times, and weather-dependent features.

Coordinated control in VPP has been much less studied than in microgrids. However, research directions can be found in both fields for researchers.

D. CONTROL BASED ON COMPLEX FREQUENCY CONCEPT

The concept of Complex Frequency (CF) was first proposed in [183]. It associates active and reactive power with voltage magnitude and phase angle. In this regard, it encapsulates the multivariable nature of power systems [75]. The real part of the complex frequency represents the change in voltage magnitude, while the imaginary part represents the change in phase angle. The magnitude of the complex frequency allows obtaining the local frequency deviation arising from both the change in phase angle and the variation in bus voltage magnitude and current injection [71].

The steady-state and transient behaviors of various types of converters have been extensively studied in the literature. However, the contribution of the controller associated with each converter at the PCC was not scrutinized. In [71], the concept of complex frequency was used to address this gap by examining the effect of each controller on the frequency at the converters' connection point.

Modeling and control with complex frequency will be very useful in future studies to examine the effect of each source on frequency, especially in systems containing multiple power sources.

E. CROSS-FORMING CONTROL

GFM methods form voltage magnitude-and-angle, while GFL methods form current magnitude-and-angle. The novel concept called ''cross-forming'', which forms voltage angle and current magnitude, was proposed by [110]. The cross-forming concept combines device security needs for fault current limitation with grid code requirements for preserving voltage angle formation, unlike pure GFM or GFL paradigms. Reference [110] introduced two viable cross-forming control implementations, allowing inverters to promptly restrict fault currents to a specified level while maintaining voltage angle forming property for GFM synchronization and dynamic ancillary services provision, during both symmetrical and asymmetrical FRT scenarios.

VI. CONCLUSION

In summary, this study provides a comprehensive review of the current literature pertaining to the control of grid-connected converters, with a particular emphasis on GFM-type control structures. The investigation spanned various aspects, including control strategies, objectives, and the evolving perspective of control techniques. Existing grid-connected control methods were reviewed in detail, their differences in terms of modeling and control were revealed, and their superior features were emphasized. The objectives of control processes were thoroughly examined, shedding

light on their critical roles in grid stability, protection, black start, and renewable energy integration. A range of practical GFM applications are showcased, encompassing real-world implementations, spanning across transmission, distribution, microgrids, and HVDC systems. It has been concluded that applications of GFM control are generally installed at the transmission level and in microgrids. It has been observed that BESS technology is mostly installed in transmission-level applications and hybrid systems are generally applied in microgrids. In conclusion, this study highlights the contemporary challenges regarding control of grid-connected systems as follows. Although classical control techniques such as droop control and VSG control provide sufficient results in small networks and under small disturbances, as the system structure becomes more complex, advanced control approaches are needed to increase system stability due to some emerging problems such as the interaction of units with each other, limited information about other units in the system and the decrease in inertia. The proposed advanced control approaches for future studies include, but are not limited to:

1) use of hybridization approaches combining positive features of control methods;
2) the realization of MIMO system models and control, which increases the control bandwidth and enables holistic control of the system, apart from the classical SISO control design;
3) coordinated control of resources, especially in a decentralized structure, in applications such as microgrids and especially virtual power plants;
4) investigating control possibilities using new modeling approaches such as complex frequency;
5) cross-forming control that establishes the voltage angle and current magnitude and allows effective current limiting.

In addition, model reduction and black and gray box modeling approaches are topics worth researching.

REFERENCES

[1] M. G. Dozein, B. C. Pal, and P. Mancarella, "Dynamics of inverter-based resources in weak distribution grids," *IEEE Trans. Power Syst.*, vol. 37, no. 5, pp. 3682–3692, Sep. 2022.

[2] H. Bevrani, H. Golpra, A. R. Messina, N. Hatziargyriou, F. Milano, and T. Ise, "Power system frequency control: An updated review of current solutions and new challenges," *Electr. Power Syst. Res.*, vol. 194, Dec. 2020, Art. no. 107114.

[3] J. Matevosyan and J. MacDowell, *Grid-Forming Technology in Energy Systems Integration*. Reston, VA, USA: Energy Systems Integration Group (ESIG), 2022.

[4] A. Tayyebi, D. Groß, A. Anta, F. Kupzog, and F. Dörfler, "Frequency stability of synchronous machines and grid-forming power converters," *IEEE J. Emerg. Sel. Topics Power Electron.*, vol. 8, no. 2, pp. 1004–1018, Jun. 2020.

[5] X. Gao, D. Zhou, A. Anvari-Moghaddam, and F. Blaabjerg, "Grid-following and grid-forming control in power electronic based power systems: A comparative study," in *Proc. IECON 47th Annu. Conf. IEEE Ind. Electron. Soc.*, Toronto, ON, Canada, Oct. 2021, pp. 1–6.

[6] R. Rosso, X. Wang, M. Liserre, X. Lu, and S. Engelken, "Grid-forming converters: Control approaches, grid-synchronization, and future trends—A review," *IEEE Open J. Ind. Appl.*, vol. 2, pp. 93–109, 2021.

[7] D. B. Rathnayake, M. Akrami, C. Phurailatpam, S. P. Me, S. Hadavi, G. Jayasinghe, S. Zabihi, and B. Bahrani, "Grid forming inverter modeling, control, and applications," *IEEE Access*, vol. 9, pp. 114781–114807, 2021.

[8] H. Zhang, W. Xiang, W. Lin, and J. Wen, "Grid forming converters in renewable energy sources dominated power grid: Control strategy, stability, application, and challenges," *J. Mod. Power Syst. Clean Energy*, vol. 9, no. 6, pp. 1239–1256, Nov. 2021.

[9] L. Xiong, X. Liu, Y. Liu, and F. Zhuo, "Modeling and stability issues of voltage-source converter-dominated power systems: A review," *CSEE J. Power Energy Syst.*, vol. 8, no. 6, pp. 1530–1549, Nov. 2022.

[10] Z. Zou, J. Tang, X. Wang, Z. Wang, W. Chen, G. Buticchi, and M. Liserre, "Modeling and control of a two-bus system with grid-forming and grid-following converters," *IEEE J. Emerg. Sel. Topics Power Electron.*, vol. 10, no. 6, pp. 7133–7149, Dec. 2022.

[11] X. Wang, M. G. Taul, H. Wu, Y. Liao, F. Blaabjerg, and L. Harnefors, "Grid-synchronization stability of converter-based resources—An overview," *IEEE Open J. Ind. Appl.*, vol. 1, pp. 115–134, 2020.

[12] C. Shah, J. D. Vasquez-Plaza, D. D. Campo-Ossa, J. F. Patarroyo-Montenegro, N. Guruwacharya, N. Bhujel, R. D. Trevizan, F. A. Rengifo, M. Shirazi, R. Tonkoski, R. Wies, T. M. Hansen, and P. Cicilio, "Review of dynamic and transient modeling of power electronic converters for converter dominated power systems," *IEEE Access*, vol. 9, pp. 82094–82117, 2021.

[13] H. Pishbahar, F. Blaabjerg, and H. Saboori, "Emerging grid-forming power converters for renewable energy and storage resources integration—A review," *Sustain. Energy Technol. Assessments*, vol. 60, Dec. 2023, Art. no. 103538.

[14] W. Liu, T. Kerekes, T. Dragicevic, and R. Teodorescu, "Review of grid stability assessment based on AI and a new concept of converter-dominated power system state of stability assessment," *IEEE J. Emerg. Sel. Topics Ind. Electron.*, vol. 4, no. 3, pp. 928–938, Jan. 2023.

[15] B. Shakerighadi, N. Johansson, R. Eriksson, P. Mitra, A. Bolzoni, A. Clark, and H. Nee, "An overview of stability challenges for power-electronic-dominated power systems: The grid-forming approach," *IET Gener., Transmiss. Distrib.*, vol. 17, no. 2, pp. 284–306, Jan. 2023.

[16] R. Musca, A. Vasile, and G. Zizzo, "Grid-forming converters. A critical review of pilot projects and demonstrators," *Renew. Sustain. Energy Rev.*, vol. 165, Sep. 2022, Art. no. 112551.

[17] B. Muftau and M. Fazeli, "The role of virtual synchronous machines in future power systems: A review and future trends," *Electr. Power Syst. Res.*, vol. 206, May 2022, Art. no. 107775.

[18] G. Song, B. Cao, and L. Chang, "Review of grid-forming inverters in support of power system operation," *Chin. J. Electr. Eng.*, vol. 8, no. 1, pp. 1–15, Mar. 2022.

[19] B. Fan, T. Liu, F. Zhao, H. Wu, and X. Wang, "A review of current-limiting control of grid-forming inverters under symmetrical disturbances," *IEEE Open J. Power Electron.*, vol. 3, pp. 955–969, 2022.

[20] A. Arasteh, L. Zeni, and N. A. Cutululis, "Fault ride through capability of grid forming wind turbines: A comparison of three control schemes," *IET Renew. Power Gener.*, vol. 16, no. 9, pp. 1866–1881, Jul. 2022.

[21] A. Alassi, K. Ahmed, A. Egea-Alvarez, and O. Ellabban, "Performance evaluation of four grid-forming control techniques with soft black-start capabilities," in *Proc. 9th Int. Conf. Renew. Energy Res. Appl. (ICRERA)*, Sep. 2020, pp. 221–226.

[22] K. V. Kkuni, S. Mohan, G. Yang, and W. Xu, "Comparative assessment of typical control realizations of grid forming converters based on their voltage source behaviour," *Energy Rep.*, vol. 9, pp. 6042–6062, Dec. 2023.

[23] U. B. Tayab, M. A. B. Roslan, L. J. Hwai, and M. Kashif, "A review of droop control techniques for microgrid," *Renew. Sustain. Energy Rev.*, vol. 76, pp. 717–727, Sep. 2017.

[24] M. Chen, D. Zhou, and F. Blaabjerg, "Modelling, implementation, and assessment of virtual synchronous generator in power systems," *J. Modern Power Syst. Clean Energy*, vol. 8, no. 3, pp. 399–411, 2020.

[25] V. Mallemaci, F. Mandrile, S. Rubino, A. Mazza, E. Carpaneto, and R. Bojoi, "A comprehensive comparison of virtual synchronous generators with focus on virtual inertia and frequency regulation," *Electr. Power Syst. Res.*, vol. 201, Dec. 2021, Art. no. 107516.

[26] K. M. Cheema, "A comprehensive review of virtual synchronous generator," *Int. J. Electr. Power Energy Syst.*, vol. 120, Sep. 2020, Art. no. 106006.

[27] M. Lu, S. Dhople, and B. Johnson, "Benchmarking nonlinear oscillators for grid-forming inverter control," *IEEE Trans. Power Electron.*, vol. 37, no. 9, pp. 10250–10266, Sep. 2022.

[28] S. A. Aghdam and M. Agamy, "Virtual oscillator-based methods for grid-forming inverter control: A review," *IET Renew. Power Gener.*, vol. 16, no. 5, pp. 835–855, Apr. 2022.

[29] Y. Teng, W. Deng, W. Pei, Y. Li, L. Dingv, and H. Ye, "Review on grid-forming converter control methods in high-proportion renewable energy power systems," *Global Energy Interconnection*, vol. 5, no. 3, pp. 328–342, Jun. 2022.

[30] K. R. Vasudevan, V. K. Ramachandaramurthy, T. S. Babu, and A. Pouryekta, "Synchronverter: A comprehensive review of modifications, stability assessment, applications and future perspectives," *IEEE Access*, vol. 8, pp. 131565–131589, 2020.

[31] B. Bahrani, M. H. Ravanji, B. Kroposki, D. Ramasubramanian, X. Guillaud, T. Prevost, and N.-A. Cutululis, "Grid-forming inverter-based resource research landscape: Understanding the key assets for renewable-rich power systems," *IEEE Power Energy Mag.*, vol. 22, no. 2, pp. 18–29, Mar. 2024.

[32] J. Rocabert, A. Luna, F. Blaabjerg, and P. Rodríguez, "Control of power converters in AC microgrids," *IEEE Trans. Power Electron.*, vol. 27, no. 11, pp. 4734–4749, Nov. 2012.

[33] B. Pawar, E. I. Batzelis, S. Chakrabarti, and B. C. Pal, "Grid-forming control for solar PV systems with power reserves," *IEEE Trans. Sustain. Energy*, vol. 12, no. 4, pp. 1947–1959, Oct. 2021.

[34] M. G. Judewicz, S. A. Gonzalez, J. R. Fischer, J. F. Martinez, and D. O. Carrica, "Inverter-side current control of grid-connected voltage source inverters with LCL filter based on generalized predictive control," *IEEE J. Emerg. Sel. Topics Power Electron.*, vol. 6, no. 4, pp. 1732–1743, Dec. 2018.

[35] H. A. Hamed, A. F. Abdou, S. Acharya, M. S. El Moursi, and E. E. EL-Kholy, "A novel dynamic switching table based direct power control strategy for grid connected converters," *IEEE Trans. Energy Convers.*, vol. 33, no. 3, pp. 1086–1097, Sep. 2018.

[36] M. A. Hannan, Z. A. Ghani, A. Mohamed, and M. N. Uddin, "Real-time testing of a fuzzy-logic-controller-based grid-connected photovoltaic inverter system," *IEEE Trans. Ind. Appl.*, vol. 51, no. 6, pp. 4775–4784, Nov. 2015.

[37] D. Chen, J. Zhang, and Z. Qian, "An improved repetitive control scheme for grid-connected inverter with frequency-adaptive capability," *IEEE Trans. Ind. Electron.*, vol. 60, no. 2, pp. 814–823, Feb. 2013.

[38] X. Fu and S. Li, "Control of single-phase grid-connected converters with LCL filters using recurrent neural network and conventional control methods," *IEEE Trans. Power Electron.*, vol. 31, no. 7, pp. 5354–5364, Jul. 2016.

[39] North American Electric Reliability Corporation, Atlanta, GA, USA. (2021). *Grid Forming Technology Bulk Power System Reliability Considerations*. [Online]. Available: https://www.nerc.com/comm/RSTC_Reliability_Guidelines/White_Paper_Grid_Forming_Technology.pdf

[40] U. Markovic, O. Stanojev, P. Aristidou, E. Vrettos, D. Callaway, and G. Hug, "Understanding small-signal stability of low-inertia systems," *IEEE Trans. Power Syst.*, vol. 36, no. 5, pp. 3997–4017, Sep. 2021.

[41] H. Han, X. Hou, J. Yang, J. Wu, M. Su, and J. M. Guerrero, "Review of power sharing control strategies for islanding operation of AC microgrids," *IEEE Trans. Smart Grid*, vol. 7, no. 1, pp. 200–215, Jan. 2016.

[42] Z. Li, K. W. Chan, J. Hu, and J. M. Guerrero, "Adaptive droop control using adaptive virtual impedance for microgrids with variable PV outputs and load demands," *IEEE Trans. Ind. Electron.*, vol. 68, no. 10, pp. 9630–9640, Oct. 2021.

[43] H.-P. Beck and R. Hesse, "Virtual synchronous machine," in *Proc. 9th Int. Conf. Elect. Power Qual. Utilisation*, Barcelona, Spain: IEEE Press, Oct. 2007, doi: 10.1109/EPQU.2007.4424220.

[44] J. Driesen and K. Visscher, "Virtual synchronous generators," in *Proc. IEEE Power Energy Soc. Gen. Meeting Convers. Del. Electr. Energy 21st Century*, Jul. 2008, pp. 1–3.

[45] R. Ofir, U. Markovic, P. Aristidou, and G. Hug, "Droop vs. Virtual inertia: Comparison from the perspective of converter operation mode," in *Proc. IEEE Int. Energy Conf. (ENERGYCON)*, Jun. 2018, pp. 1–6.

[46] Y. Du, J. M. Guerrero, L. Chang, J. Su, and M. Mao, "Modeling, analysis, and design of a frequency-droop-based virtual synchronous generator for microgrid applications," in *Proc. IEEE ECCE Asia Downunder*, Jun. 2013, pp. 643–649.

[47] N. Mohammed, M. H. Ravanji, W. Zhou, and B. Bahrani, "Online grid impedance estimation-based adaptive control of virtual synchronous generators considering strong and weak grid conditions," *IEEE Trans. Sustain. Energy*, vol. 14, no. 1, pp. 673–687, Jan. 2023.

[48] L. Zhang, L. Harnefors, and H.-P. Nee, "Power-synchronization control of grid-connected voltage-source converters," *IEEE Trans. Power Syst.*, vol. 25, no. 2, pp. 809–820, May 2010.

[49] M. Chen, D. Zhou, A. Tayyebi, E. Prieto-Araujo, F. Dörfler, and F. Blaabjerg, "Generalized multivariable grid-forming control design for power converters," *IEEE Trans. Smart Grid*, vol. 13, no. 4, pp. 2873–2885, Jul. 2022.

[50] J. C. Vasquez, J. M. Guerrero, M. Savaghebi, J. Eloy-Garcia, and R. Teodorescu, "Modeling, analysis, and design of stationary-reference-frame droop-controlled parallel three-phase voltage source inverters," *IEEE Trans. Ind. Electron.*, vol. 60, no. 4, pp. 1271–1280, Apr. 2013.

[51] W. Zhang, D. Remon, and P. Rodriguez, "Frequency support characteristics of grid-interactive power converters based on the synchronous power controller," *IET Renew. Power Gener.*, vol. 11, no. 4, pp. 470–479, Mar. 2017.

[52] L. Harnefors, M. Hinkkanen, U. Riaz, F. M. M. Rahman, and L. Zhang, "Robust analytic design of power-synchronization control," *IEEE Trans. Ind. Electron.*, vol. 66, no. 8, pp. 5810–5819, Aug. 2019.

[53] J. F. Morris, K. H. Ahmed, and A. Egea-Àlvarez, "Power-synchronization control for ultra-weak AC networks: Comprehensive stability and dynamic performance assessment," *IEEE Open J. Ind. Electron. Soc.*, vol. 2, pp. 441–450, 2021.

[54] Q.-C. Zhong and G. Weiss, "Synchronverters: Inverters that mimic synchronous generators," *IEEE Trans. Ind. Electron.*, vol. 58, no. 4, pp. 1259–1267, Apr. 2011.

[55] Z. Kustanovich, S. Shivratri, H. Yin, F. Reissner, and G. Weiss, "Synchronverters with fast current loops," *IEEE Trans. Ind. Electron.*, vol. 70, no. 11, pp. 11357–11367, Nov. 2023.

[56] Z. Kustanovich, F. Reissner, S. Shivratri, and G. Weiss, "The sensitivity of grid-connected synchronverters with respect to measurement errors," *IEEE Access*, vol. 9, pp. 118985–118995, 2021.

[57] S. Pola, M. A. Azzouz, and M. Mirhassani, "Synchronverters with fault ride-through capabilities for reliable microgrid protection during balanced and unbalanced faults," *IEEE Trans. Sustain. Energy*, vol. 15, no. 3, pp. 1663–1676, Jul. 2024.

[58] T. Jouini, C. Arghir, and F. Drfler, "Grid-friendly matching of synchronous machines by tapping into the DC storage," *IFAC-PapersOnLine*, vol. 49, no. 22, pp. 192–197, Jan. 2016.

[59] C. Arghir, T. Jouini, and F. Dörfler, "Grid-forming control for power converters based on matching of synchronous machines," *Automatica*, vol. 95, pp. 273–282, Sep. 2018.

[60] C. Arghir and F. Dörfler, "The electronic realization of synchronous machines: Model matching, angle tracking, and energy shaping techniques," *IEEE Trans. Power Electron.*, vol. 35, no. 4, pp. 4398–4410, Apr. 2020.

[61] S. Curi, D. Groß, and F. Dörfler, "Control of low-inertia power grids: A model reduction approach," in *Proc. IEEE 56th Annu. Conf. Decis. Control (CDC)*, Dec. 2017, pp. 5708–5713.

[62] T. Qoria, E. Rokrok, A. Bruyere, B. François, and X. Guillaud, "A PLL-free grid-forming control with decoupled functionalities for high-power transmission system applications," *IEEE Access*, vol. 8, pp. 197363–197378, 2020.

[63] B. B. Johnson, S. V. Dhople, A. O. Hamadeh, and P. T. Krein, "Synchronization of parallel single-phase inverters with virtual oscillator control," *IEEE Trans. Power Electron.*, vol. 29, no. 11, pp. 6124–6138, Nov. 2014.

[64] B. B. Johnson, M. Sinha, N. G. Ainsworth, F. Dörfler, and S. V. Dhople, "Synthesizing virtual oscillators to control islanded inverters," *IEEE Trans. Power Electron.*, vol. 31, no. 8, pp. 6002–6015, Aug. 2016.

[65] M. Sinha, F. Dörfler, B. B. Johnson, and S. V. Dhople, "Uncovering droop control laws embedded within the nonlinear dynamics of van der pol oscillators," *IEEE Trans. Control Netw. Syst.*, vol. 4, no. 2, pp. 347–358, Jun. 2017.

[66] J. Li, M. Ali, J. E. Fletcher, and H. I. Nurdin, "Modeling and analysis of multiple inverters with dual-loop-based virtual oscillator control," *IEEE J. Emerg. Sel. Topics Power Electron.*, vol. 10, no. 4, pp. 3963–3974, Aug. 2022.

[67] M. Colombino, D. Groß, and F. Dörfler, "Global phase and voltage synchronization for power inverters: A decentralized consensus-inspired approach," in *Proc. IEEE 56th Annu. Conf. Decis. Control (CDC)*, Dec. 2017, pp. 5690–5695.

[68] M. Colombino, D. Groz, J.-S. Brouillon, and F. Dorfler, "Global phase and magnitude synchronization of coupled oscillators with application to the control of grid-forming power inverters," *IEEE Trans. Autom. Control*, vol. 64, no. 11, pp. 4496–4511, Nov. 2019.

[69] M. A. Awal and I. Husain, "Unified virtual oscillator control for grid-forming and grid-following converters," *IEEE J. Emerg. Sel. Topics Power Electron.*, vol. 9, no. 4, pp. 4573–4586, Aug. 2021.

[70] U. Markovic, *Towards Reliable Operation of Converter-dominated Power Systems: Dynamics, Optimization and Control*. Zürich, Switzerland: ETH Zürich, 2020.

[71] D. Moutevelis, J. Roldán-Pérez, M. Prodanovic, and F. Milano, "Taxonomy of power converter control schemes based on the complex frequency concept," *IEEE Trans. Power Syst.*, vol. 39, no. 1, pp. 1996–2009, Sep. 2024.

[72] W. Du, Z. Chen, K. P. Schneider, R. H. Lasseter, S. Pushpak Nandanoori, F. K. Tuffner, and S. Kundu, "A comparative study of two widely used grid-forming droop controls on microgrid small-signal stability," *IEEE J. Emerg. Sel. Topics Power Electron.*, vol. 8, no. 2, pp. 963–975, Jun. 2020.

[73] Q.-C. Zhong, Y. Wang, and B. Ren, "UDE-based robust droop control of inverters in parallel operation," *IEEE Trans. Ind. Electron.*, vol. 64, no. 9, pp. 7552–7562, Sep. 2017.

[74] A. Tayyebi, A. Magdaleno, D. Vettoretti, M. Chen, E. Prieto-Araujo, A. Anta, and F. Dörfler, "System-level performance and robustness of the grid-forming hybrid angle control," *Electr. Power Syst. Res.*, vol. 212, Nov. 2022, Art. no. 108503.

[75] X. He, V. Häberle, and F. Dörfler, "Complex-frequency synchronization of converter-based power systems," *IEEE Trans. Control Netw. Syst.*, early access, Jul. 1, 2024, doi: 10.1109/TCNS.2024.3420983.

[76] M. A. Awal, M. R. K. Rachi, H. Yu, I. Husain, and S. Lukic, "Double synchronous unified virtual oscillator control for asymmetrical fault ride-through in grid-forming voltage source converters," *IEEE Trans. Power Electron.*, vol. 38, no. 6, pp. 6759–6763, Jun. 2023.

[77] J. Liu, Y. Miura, and T. Ise, "Comparison of dynamic characteristics between virtual synchronous generator and droop control in inverter-based distributed generators," *IEEE Trans. Power Electron.*, vol. 31, no. 5, pp. 3600–3611, May 2016.

[78] *IEEE Standard for Interconnection and Interoperability of Distributed Energy Resources with Associated Electric Power Systems Interfaces*, Standard 1547-2018, 2018.

[79] *IEEE Standard for Interconnection and Interoperability of Inverter-Based Resources (IBRs) Interconnecting with Associated Transmission Electric Power Systems*, Standard 2800-2022, 2022.

[80] T. Qoria, *Grid-Forming Control to Achieve a 100% Power Electronics Interfaced Power Transmission Systems*. Paris, France: HESAM Universit, 2020.

[81] S. D'Arco, J. A. Suul, and O. B. Fosso, "A virtual synchronous machine implementation for distributed control of power converters in SmartGrids," *Electr. Power Syst. Res.*, vol. 122, pp. 180–197, May 2015.

[82] M. Chen, D. Zhou, A. Tayyebi, E. Prieto-Araujo, F. Dorfler, and F. Blaabjerg, "On power control of grid-forming converters: Modeling, controllability, and full-state feedback design," *IEEE Trans. Sustain. Energy*, vol. 15, no. 1, pp. 68–80, Jan. 2024.

[83] D. B. Rathnayake and B. Bahrani, "Multivariable control design for grid-forming inverters with decoupled active and reactive power loops," *IEEE Trans. Power Electron.*, vol. 38, no. 2, pp. 1635–1649, Feb. 2023.

[84] N. Hoffmann and F. W. Fuchs, "Minimal invasive equivalent grid impedance estimation in inductive–resistive power networks using extended Kalman filter," *IEEE Trans. Power Electron.*, vol. 29, no. 2, pp. 631–641, Feb. 2014.

[85] S. Cobreces, E. J. Bueno, D. Pizarro, F. J. Rodriguez, and F. Huerta, "Grid impedance monitoring system for distributed power generation electronic interfaces," *IEEE Trans. Instrum. Meas.*, vol. 58, no. 9, pp. 3112–3121, Sep. 2009.

[86] M. Ciobotaru, V. Agelidis, and R. Teodorescu, "Line impedance estimation using model based identification technique," in *Proc. 14th Eur. Conf. Power Electron. Appl.*, Aug. 2011, pp. 1–9.

[87] N. Mohammed, T. Kerekes, and M. Ciobotaru, "An online event-based grid impedance estimation technique using grid-connected inverters," *IEEE Trans. Power Electron.*, vol. 36, no. 5, pp. 6106–6117, May 2021.

[88] L. Asiminoaei, R. Teodorescu, F. Blaabjerg, and U. Borup, "Implementation and test of an online embedded grid impedance estimation technique for PV inverters," *IEEE Trans. Ind. Electron.*, vol. 52, no. 4, pp. 1136–1144, Aug. 2005.

[89] T. Roinila, T. Messo, and A. Aapro, "Impedance measurement of three phase systems in DQ-domain: Applying MIMO-identification techniques," in *Proc. IEEE Energy Convers. Congr. Expo. (ECCE)*, Sep. 2016, pp. 1–6.

[90] M. Céspedes and J. Sun, "Online grid impedance identification for adaptive control of grid-connected inverters," in *Proc. IEEE Energy Convers. Congr. Expo. (ECCE)*, Sep. 2012, pp. 914–921.

[91] N. Mohammed and M. Ciobotaru, "Fast and accurate grid impedance estimation approach for stability analysis of grid-connected inverters," *Electr. Power Syst. Res.*, vol. 207, Jun. 2022, Art. no. 107831.

[92] *IEEE Guide for Planning DC Links Terminating at AC Locations Having Low Short-Circuit Capacities*, Standard 1204-1997, 1997.

[93] J. Z. Zhou, H. Ding, S. Fan, Y. Zhang, and A. M. Gole, "Impact of short-circuit ratio and phase-locked-loop parameters on the small-signal behavior of a VSC-HVDC converter," *IEEE Trans. Power Del.*, vol. 29, no. 5, pp. 2287–2296, Oct. 2014.

[94] S.-K. Chung, "A phase tracking system for three phase utility interface inverters," *IEEE Trans. Power Electron.*, vol. 15, no. 3, pp. 431–438, May 2000.

[95] G. S. Misyris, J. A. Mermet-Guyennet, S. Chatzivasileiadis, and T. Weckesser, "Grid supporting VSCs in power systems with varying inertia and short-circuit capacity," in *Proc. IEEE Milan PowerTech*, Jun. 2019, pp. 1–6.

[96] U. Markovic, J. Vorwerk, P. Aristidou, and G. Hug, "Stability analysis of converter control modes in low-inertia power systems," in *Proc. IEEE PES Innov. Smart Grid Technol. Conf. Eur. (ISGT-Eur.)*, Oct. 2018, pp. 1–6.

[97] U. Markovic, O. Stanojev, P. Aristidou, and G. Hug, "Partial grid forming concept for 100% inverter-based transmission systems," in *Proc. IEEE Power Energy Soc. Gen. Meeting (PESGM)*, Aug. 2018, pp. 1–5.

[98] R. Rosso, J. Cassoli, G. Buticchi, S. Engelken, and M. Liserre, "Robust stability analysis of LCL filter based synchronverter under different grid conditions," *IEEE Trans. Power Electron.*, vol. 34, no. 6, pp. 5842–5853, Jun. 2019.

[99] R. Rosso, S. Engelken, and M. Liserre, "Robust stability analysis of synchronverters operating in parallel," *IEEE Trans. Power Electron.*, vol. 34, no. 11, pp. 11309–11319, Nov. 2019.

[100] R. Pan, S. Liu, H. Gu, D. Liu, L. Zhu, and E. Chen, "Stability analysis of hybrid synchronization controller based grid forming control," *Energy Rep.*, vol. 9, pp. 1291–1298, Oct. 2023.

[101] N. Hatziargyriou, J. V. Milanović, C. Rahmann, V. Ajjarapu, C. Cañizares, I. Erlich, D. Hill, I. Hiskens, I. Kamwa, B. Pal, P. Pourbeik, J. J. Sanchez-Gasca, A. Stanković, T. Van Cutsem, V. Vittal, and C. Vournas, "Stability definitions and characterization of dynamic behavior in systems with high penetration of power electronic interfaced technologies," IEEE Power Energy Soc., Tech. Rep. PES-TR77, Sep. 2020.

[102] N. Hatziargyriou, J. Milanovic, C. Rahmann, V. Ajjarapu, C. Canizares, I. Erlich, D. Hill, I. Hiskens, I. Kamwa, B. Pal, P. Pourbeik, J. Sanchez-Gasca, A. Stankovic, T. Van Cutsem, V. Vittal, and C. Vournas, "Definition and classification of power system stability—Revisited & extended," *IEEE Trans. Power Syst.*, vol. 36, no. 4, pp. 3271–3281, Jul. 2021.

[103] A. Shrestha and F. Gonzalez-Longatt, "Frequency stability issues and research opportunities in converter dominated power system," *Energies*, vol. 14, no. 14, p. 4184, Jul. 2021.

[104] P. S. Kundur, *Power System Stability and Control*, 1st ed., New York, NY, USA: McGraw-Hill, 1994.

[105] X. Gao, D. Zhou, A. Anvari-Moghaddam, and F. Blaabjerg, "Stability analysis of grid-following and grid-forming converters based on state-space modelling," *IEEE Trans. Ind. Appl.*, vol. 60, no. 3, pp. 4910–4920, May 2024.

[106] X. Xiong, C. Wu, B. Hu, D. Pan, and F. Blaabjerg, "Transient damping method for improving the synchronization stability of virtual synchronous generators," *IEEE Trans. Power Electron.*, vol. 36, no. 7, pp. 7820–7831, Jul. 2021.

[107] D. Groß, M. Colombino, J.-S. Brouillon, and F. Dörfler, "The effect of transmission-line dynamics on grid-forming dispatchable virtual oscillator control," *IEEE Trans. Control Netw. Syst.*, vol. 6, no. 3, pp. 1148–1160, Sep. 2019.

[108] B. Wang, R. Burgos, and B. Wen, "Grid-forming inverter control strategy with improved fault ride through capability," in *Proc. IEEE Energy Convers. Congr. Expo.*, Oct. 2022, pp. 1–8.

[109] M. G. Taul, X. Wang, P. Davari, and F. Blaabjerg, "Current limiting control with enhanced dynamics of grid-forming converters during fault conditions," *IEEE J. Emerg. Sel. Topics Power Electron.*, vol. 8, no. 2, pp. 1062–1073, Jun. 2020.

[110] X. He, M. A. Desai, L. Huang, and F. Dörfler, "Cross-forming control and fault current limiting for grid-forming inverters," Apr. 2024, *arXiv:2404.13376*.

[111] E. Pajuelo, R. Gokaraju, and M. S. Sachdev, "Coordination of overexcitation limiter, field overcurrent protection and generator control," in *Proc. IEEE PES General Meeting*, Jul. 2010, pp. 1–7.

[112] M. E. Baran and N. R. Mahajan, "Overcurrent protection on voltage-source-converter-based multiterminal DC distribution systems," *IEEE Trans. Power Del.*, vol. 22, no. 1, pp. 406–412, Jan. 2007.

[113] P. M. Anderson, *Power System Protection*. New York, NY, USA: IEEE Press, 1999.

[114] J. Jia, G. Yang, and A. H. Nielsen, "A review on grid-connected converter control for short-circuit power provision under grid unbalanced faults," *IEEE Trans. Power Del.*, vol. 33, no. 2, pp. 649–661, Apr. 2018.

[115] T. Qoria, X. Wang, and R. Kadri, "Grid-forming control VSC-based including current limitation and re-synchronization functions to deal with symmetrical and asymmetrical faults," *Electr. Power Syst. Res.*, vol. 223, Oct. 2023, Art. no. 109647.

[116] G. Denis, T. Prevost, M. Debry, F. Xavier, X. Guillaud, and A. Menze, "The migrate project: The challenges of operating a transmission grid with only inverter-based generation. A grid-forming control improvement with transient current-limiting control," *IET Renew. Power Gener.*, vol. 12, no. 5, pp. 523–529, Apr. 2018.

[117] A. Gkountaras, S. Dieckerhoff, and T. Sezi, "Evaluation of current limiting methods for grid forming inverters in medium voltage microgrids," in *Proc. IEEE Energy Convers. Congr. Expo.*, Oct. 2015, pp. 1223–1230.

[118] A. D. Paquette and D. M. Divan, "Virtual impedance current limiting for inverters in microgrids with synchronous generators," *IEEE Trans. Ind. Appl.*, vol. 51, no. 2, pp. 1630–1638, Mar. 2015.

[119] X. Wang, Y. W. Li, F. Blaabjerg, and P. C. Loh, "Virtual-impedance-based control for voltage-source and current-source converters," *IEEE Trans. Power Electron.*, vol. 30, no. 12, pp. 7019–7037, Dec. 2015.

[120] Q.-C. Zhong and G. C. Konstantopoulos, "Current-limiting droop control of grid-connected inverters," *IEEE Trans. Ind. Electron.*, vol. 64, no. 7, pp. 5963–5973, Jul. 2017.

[121] I. Sadeghkhani, M. E. H. Golshan, J. M. Guerrero, and A. Mehrizi-Sani, "A current limiting strategy to improve fault ride-through of inverter interfaced autonomous microgrids," *IEEE Trans. Smart Grid*, vol. 8, no. 5, pp. 2138–2148, Sep. 2017.

[122] H. Xin, L. Huang, L. Zhang, Z. Wang, and J. Hu, "Synchronous instability mechanism of P-f droop-controlled voltage source converter caused by current saturation," *IEEE Trans. Power Syst.*, vol. 31, no. 6, pp. 5206–5207, Nov. 2016.

[123] J. He and Y. W. Li, "Analysis, design, and implementation of virtual impedance for power electronics interfaced distributed generation," *IEEE Trans. Ind. Appl.*, vol. 47, no. 6, pp. 2525–2538, Nov. 2011.

[124] Q. Taoufik, H. Wu, X. Wang, and I. Colak, "Variable virtual impedance-based overcurrent protection for grid-forming inverters: Small-signal, large-signal analysis and improvement," *IEEE Trans. Smart Grid*, vol. 14, no. 5, pp. 3324–3336, Sep. 2023.

[125] T. Qoria, "WP3-control and operation of a grid with 100% converter-based devices. deliverable 3.2: Local control and simulation tools for large transmission systems," MIGRATE Project, Eur. Union, Tech. Rep., 2018. [Online]. Available: https://d1wqtxts1xzle7.cloudfront.net/91077452/D3.2_20-_20Local_20control_20and_20simulation_20tools_20for_20large_20transmission_20systems-libre.pdf?1663231152=&response-content-disposition=inline%3B+filename%3DWP_3_Control_and_Operation_of_a_Grid_wit.pdf&Expires=1722678941&Signature=NOlJac8rr59n4p6aV0zPQHMaVBgU8dvWtu3Aq~mvhVdJwzB40TPeFLJQ6SASGQhkE3btXfUyeZIXZU6vkPPJREaNRyqJX4o4lZ0kRtg1E5t8Bs1Xfj9JHbFqg77r6dVNyIupuvn1C6SnuUGvnsxg-eUeQEY7W~Z2674gdpkjplGFNV~W7dTJmFrRucrwGhHyvz7SMsWDKFXe7m8JPV~dZRXRktuD07SeZ-FEKe0JUgyJRYjs~IPnzR9O1nbFpGCUpVyjBWZ5Sono~xNGftj9K4ncz2PQ~Zw1IW0s9nF-Q5B8E5taEfJAnq00jMhKjNbFvu3YBW2l7bpKJvMtNCZYwg__&Key-Pair-Id=APKAJLOHF5GGSLRBV4ZA

[126] E. Rokrok, T. Qoria, A. Bruyere, B. Francois, and X. Guillaud, "Transient stability assessment and enhancement of grid-forming converters embedding current reference saturation as current limiting strategy," *IEEE Trans. Power Syst.*, vol. 37, no. 2, pp. 1519–1531, Mar. 2022.

[127] S. Pola and M. A. Azzouz, "Optimal protection coordination of active distribution networks with synchronverters," *IEEE Access*, vol. 10, pp. 75105–75116, 2022.

[128] *Power System Restoration Accounting for a Rapidly Changing Power System and Generation Mix*, CIGRE, Paris, France, 2023.

[129] A. P. Asensio, S. A. Gómez, and J. L. Rodriguez-Amenedo, "Black-start capability of PV power plants through a grid-forming control based on reactive power synchronization," *Int. J. Electr. Power Energy Syst.*, vol. 146, Mar. 2023, Art. no. 108730.

[130] B. Kroposki, D. Ramasubramanian, W. Wang, A. Huque, J. Boemer, and A. Hoke, *UNIFI Specifications for Grid-Forming Inverter-Based Resources: Version 2*. Golden, CO, USA: National Renewable Energy Laboratory (NREL), 2024.

[131] J. G. OBrien, *Electric Grid Blackstart: Trends, Challenges, and Opportunities*. Richland, WA, USA: Pacific Northwest National Lab. (PNNL), Apr. 2022.

[132] J. L. Rodríguez-Amenedo, S. A. Gómez, J. C. Martínez, and J. Alonso-Martinez, "Black-start capability of DFIG wind turbines through a grid-forming control based on the rotor flux orientation," *IEEE Access*, vol. 9, pp. 142910–142924, 2021.

[133] C. Klauber, H. Burroughs, and A. Zhou, "Collaborative and autonomous black start: Theory and implementation," in *Proc. IEEE Power Energy Soc. Innov. Smart Grid Technol. Conf. (ISGT)*, Jan. 2023, pp. 1–5.

[134] O. Dutta, T. Chen, D. Ramasubramanian, and E. Farantatos, "Adaptive control of grid forming inverters for system black start," in *Proc. IEEE Power Energy Soc. Innov. Smart Grid Technol. Conf. (ISGT)*, Jan. 2023, pp. 1–5.

[135] A. Alassi, Z. Feng, K. Ahmed, M. Syed, A. Egea-Alvarez, and C. Foote, "Grid-forming VSM control for black-start applications with experimental PHiL validation," *Int. J. Electr. Power Energy Syst.*, vol. 151, Sep. 2023, Art. no. 109119.

[136] Y. Pan, X. Yin, Z. Zhang, B. Liu, M. Wang, and X. Yin, "Three-phase transformer inrush current reduction strategy based on prefluxing and controlled switching," *IEEE Access*, vol. 9, pp. 38961–38978, 2021.

[137] H. Saad, V. Rudan, F. Pezet, A. Verdicchio, S. Subrin, Y. Vernay, P. Nguyen, G. Postiglione, L. B. Pereira, S. Abibou, and M. Aguado, "Experience and EMT study for onsite grid forming test using BESS–RINGO black start project," in *Proc. 21st Wind Sol. Integr. Workshop (WIW)*, Oct. 2022, vol. 2022, pp. 241–249.

[138] Y. Si, N. Korada, Q. Lei, and R. Ayyanar, "A robust controller design methodology addressing challenges under system uncertainty," *IEEE Open J. Power Electron.*, vol. 3, pp. 402–418, 2022.

[139] L. Huang, H. Xin, and F. Drfler, "H_∞-control of grid-connected converters: Design, objectives and decentralized stability certificates," *IEEE Trans. Smart Grid*, vol. 11, no. 5, pp. 3805–3816, Sep. 2020.

[140] F. Sadeque, D. Sharma, and B. Mirafzal, "Seamless grid-following to grid-forming transition of inverters supplying a microgrid," in *Proc. IEEE Appl. Power Electron. Conf. Expo. (APEC)*, Mar. 2023, pp. 594–599.

[141] J. Meng, Z. Zhang, G. Zhang, T. Ye, P. Zhao, Y. Wang, J. Yang, and J. Yu, "Adaptive model predictive control for grid-forming converters to achieve smooth transition from islanded to grid-connected mode," *IET Gener., Transmiss. Distrib.*, vol. 17, no. 12, pp. 2833–2845, Jun. 2023.

[142] M. A. Awal, H. Yu, H. Tu, S. M. Lukic, and I. Husain, "Hierarchical control for virtual oscillator based grid-connected and islanded microgrids," *IEEE Trans. Power Electron.*, vol. 35, no. 1, pp. 988–1001, Jan. 2020.

[143] *PCS100 ESS High Performance Inverter For Micro-Grid Applications*, ABB Ltd. Napier, New Zealand, 2020.

[144] *Hitachi ABB Power Grids to Become Hitachi Energy*, Hitachi Eur., Buckinghamshire, U.K., 2021.

[145] *e-Mesh Powerstore Grid-Forming Battery Energy Storage System Enabling Resilient and Cost-Effective Access to Power*, Hitachi Energy Publisher, Zurich, Switzerland, 2024.

[146] *Gamesa Electric Proteus PCS-E 1500V Battery Inverters*, Gamesa Electr., Biscay, Spain, 2023.

[147] *LUNA2000-200KTL-H1 Smart PCS, Huawei*. Accessed: May 28, 2024. [Online]. Available: https://solar.huawei.com/download?p=%2F-%2Fmedia%2FSolar%2Fdatasheet%2FLUNA2000-200KTL-H1.pdf

[148] *Sunny Central Storage 1900/2200/2475/2900—Battery Inverter for Large-Scale Storage Systems, SMA Solar Technology*. Accessed: May 28, 2024. [Online]. Available: https://files.sma.de/downloads/SCS1900-2900-DS-en-20.pdf
[149] *MACH Control and Protection System | Hitachi Energy*, SMA Solar Technol. AG, Niestetal, Germany.
[150] *SVC Light Enhanced | Hitachi Energy*. Accessed: May 29, 2024. [Online]. Available: https://publisher.hitachienergy.com/preview?DocumentID=9AKK107992A6600&LanguageCode=en&DocumentPartId=&Action=Launch
[151] *SVC PLUS Frequency Stabilizer*, Siemens Energy AG, Munich, Germany.
[152] M. Koller, M. Gonzlez Vay, A. Chacko, T. Borsche, and A. Ulbig, *Primary Control Reserves Provision With Battery Energy Storage Systems in the Largest European Ancillary Services Cooperation*. Paris, France: Set Pap. CIGRE Sess. Aug. 2016.
[153] M. Koller, T. Borsche, A. Ulbig, and G. Andersson, "Review of grid applications with the Zurich 1MW battery energy storage system," *Electr. Power Syst. Res.*, vol. 120, pp. 128–135, Mar. 2015.
[154] M. Ribeiro, I. Miranda, L. Marques, and A. Bernardo, "DEMOCRAT: Demonstrator of a micro-grid integrating storage," in *Proc. CIRED Workshop*, 2018, pp. 7–8.
[155] S. Cherevatskiy, "Grid forming energy storage system addresses challenges of grids with high penetration of renewables (a case study)," in *Proc. 48th Cigre Sessions*, 2020, p. 322.
[156] O. Schmann, "Experiences with large grid-forming inverters on various island and microgrid projects," in presented at the 4th Int. Hybrid Power Syst. Workshop, Crete, Greece, May 22/23, 2019. [Online]. Available: https://hybridpowersystems.org/crete2019/wp-content/uploads/sites/13/2020/03/3A_3_HYB19_017_paper_Schoemann_Oliver.pdf and https://hybridpowersystems.org/wp-content/uploads/sites/13/2019/06/3A_3_HYB19_017_presentation_Schoemann_Oliver_web.pdf
[157] *The Bordesholm Stand-Alone Grid Ensures Power Supply Even in the Event of a Grid Failure*. Accessed: Jan. 25, 2024. [Online]. Available: https://www.sma-sunny.com/en/the-bordesholm-stand-alone/
[158] (2023). *Wrtsil and AGL Complete Construction of 250 MW Energy Storage Facility in Australia*. Accessed: Dec. 31, 2023. [Online]. Available: https://www.wartsila.com/media/news/22-08-2023-wartsila-and-agl-complete-construction-of-250-mw-energy-storage-facility-in-australia-3311991
[159] A. Roscoe, "Practical experience of operating a grid forming wind park and its response to system events," in *Proc. 18th Wind Integr. Workshop*, 219AD. [Online]. Available: : https://knowledge.rtds.com/hc/en-us/article_attachments/1500001877941
[160] W. Yan, S. Shah, V. Gevorgian, P. Koralewicz, R. Wallen, and D. W. Gao, "On the low risk of SSR in type III wind turbines operating with grid-forming control," *IEEE Trans. Sustain. Energy*, vol. 15, no. 1, pp. 443–453, Jan. 2024.
[161] *Final Report Grid Energy Storage System*, AusNet Services, Melbourne, VIC, Australia.
[162] *Hybrid Energy Storage System in Graciosa, Azores, Portugal–Wrtsil Energy*.
[163] L. Petersen, F. Iov, G. C. Tarnowski, V. Gevorgian, P. Koralewicz, and D.-I. Stroe, "Validating performance models for hybrid power plant control assessment," *Energies*, vol. 12, no. 22, p. 4330, Nov. 2019.
[164] Energy Update Magazine, Karachi, Pakistan. (2020). *GE Achieves Battery-Enabled Blackstart of Heavy Duty Gas Turbine*. Accessed: Jan. 2, 2024. [Online]. Available: https://www.energyupdate.com.pk/2020/03/07/ge-achieves-battery-enabled-blackstart-of-heavy-duty-gas-turbine/
[165] *OSMOSE Final Report*, RTE, Paris, France, 2022.
[166] M. B. Marz, "Mackinac HVDC construction and testing," presented at the Minnesota Power Syst. Conf. (MIPSYCON), MN, USA, Nov. 5, 2014. [Online]. Available: https://pdfs.semanticscholar.org/910d/47a8852aabc0c7daf0754d8f8f118e5dc3bb.pdf
[167] (2022). *Breaking Ground at Broken Hill for AGLs New Grid-Scale Battery*. Accessed: Dec. 31, 2023. [Online]. Available: https://www.agl.com.au/about-agl/media-centre/asx-and-media-releases/2022/november/breaking-ground-at-broken-hill-for-agl-s-new-grid-scale-battery
[168] *AGL Broken Hill Grid-Forming Battery*. Accessed: Jan. 25, 2024. [Online]. Available: https://arena.gov.au/projects/agl-broken-hill-grid-forming-battery/
[169] *AGL to Begin Construction of Australias Biggest 'Grid Forming Battery in 2024*. Accessed: Jan. 4, 2024. [Online]. Available: https://reneweconomy.com.au/agl-to-begin-construction-of-australias-biggest-grid-forming-battery-in-2024/
[170] *Palmerston BESS—Akaysha*. Accessed: Jan. 4, 2024. [Online]. Available: https://akayshaenergy.com/projects/palmerston-bess
[171] *Neilston Greener Grid Park*. Accessed: Jan. 4, 2024. [Online]. Available: https://projects.statkraft.co.uk/Neilston/
[172] *Coylton Greener Grid Park*. Accessed: Jan. 4, 2024. [Online]. Available: https://projects.statkraft.co.uk/coylton/
[173] *Zenob Breaks Ground on Pioneering 300MW Battery in Blackhillock Zenob*. Accessed: Jan. 4, 2024. [Online]. Available: https://www.zenobe.com/news-and-events/zenobe-breaks-ground-on-pioneering-300mw-battery-in-blackhillock/
[174] *Zenobe Starts Work on 1-GW Grid Forming Battery Portfolio in Scotland*. Accessed: Jan. 4, 2024. [Online]. Available: https://renewablesnow.com/news/zenobe-starts-work-on-1-gw-grid-forming-battery-portfolio-in-scotland-804651/
[175] M. Chen, D. Zhou, and F. Blaabjerg, "Multivariable grid-forming converters with direct states control," *IEEE Trans. Ind. Appl.*, vol. 59, no. 4, pp. 4334–4341, Jul. 2023.
[176] M. Chen, D. Zhou, A. Tayyebi, E. Prieto-Araujo, F. Dorfler, and F. Blaabjerg, "Augmentation of generalized multivariable grid-forming control for power converters with cascaded controllers," in *Proc. Int. Power Electron. Conf. (IPEC-Himeji–ECCE Asia)*, May 2022, pp. 998–1004.
[177] J. Liu, Y. Miura, H. Bevrani, and T. Ise, "A unified modeling method of virtual synchronous generator for multi-operation-mode analyses," *IEEE J. Emerg. Sel. Topics Power Electron.*, vol. 9, no. 2, pp. 2394–2409, Apr. 2021.
[178] X. Meng, J. Liu, and Z. Liu, "A generalized droop control for grid-supporting inverter based on comparison between traditional droop control and virtual synchronous generator control," *IEEE Trans. Power Electron.*, vol. 34, no. 6, pp. 5416–5438, Jun. 2019.
[179] T. Liu and X. Wang, "Unified voltage control for grid-forming inverters," *IEEE Trans. Ind. Electron.*, vol. 71, no. 3, pp. 2578–2589, Mar. 2024.
[180] J. Chen, M. Liu, and F. Milano, "Aggregated model of virtual power plants for transient frequency and voltage stability analysis," *IEEE Trans. Power Syst.*, vol. 36, no. 5, pp. 4366–4375, Sep. 2021.
[181] S. Awerbuch and A. Preston, *The Virtual Utility: Accounting, Technology & Competitive Aspects of the Emerging Industry*. Boston, MA, USA: Kluwer, 1997.
[182] V. Häberle, M. W. Fisher, E. Prieto-Araujo, and F. Dörfler, "Control design of dynamic virtual power plants: An adaptive divide-and-conquer approach," *IEEE Trans. Power Syst.*, vol. 37, no. 5, pp. 4040–4053, Sep. 2022.
[183] F. Milano, "Complex frequency," *IEEE Trans. Power Syst.*, vol. 37, no. 2, pp. 1230–1240, Mar. 2022.

MACIT TOZAK (Graduate Student Member, IEEE) received the B.Sc. degree in electrical and electronics engineering from Hacettepe University, Ankara, Türkiye, in 2013, and the M.Sc. degree from Manisa Celal Bayar University, Manisa, Türkiye, in 2020, where he is currently pursuing the Ph.D. degree with the Department of Electrical and Electronics Engineering. His research interests include modeling, control, and stability analysis of power converters.

SEZAI TASKIN received the B.Sc., M.Sc., and Ph.D. degrees from Marmara University, Istanbul, Türkiye, in 1999, 2001, and 2007, respectively. He held a visiting researcher position with Florida International University, Miami, USA, in 2013. He is currently a Professor in electrical and electronics engineering with Manisa Celal Bayar University, Türkiye. His research interests include control system applications, solar PV systems, and battery energy storage systems.

IBRAHIM SENGOR (Senior Member, IEEE) received the B.Sc. degree in electrical engineering from Istanbul Technical University (ITU), in 2013, and the M.Sc. and Ph.D. degrees in electrical engineering from Yildiz Technical University (YTU), Istanbul, Türkiye, in 2016 and 2019, respectively. He was a Research Assistant and a Teaching Assistant with the Electrical Engineering Department, YTU, during his graduate studies. He was an Assistant Professor in electrical power engineering with Izmir Katip Celebi University (IKCU), Izmir, Türkiye, between 2019 and 2022. He was a Postdoctoral Research Fellow in electrification of transport and heating within the electric power system with MaREI, the SFI Centre, University College Cork (UCC), Cork, Ireland, between June 2021 and September 2023. He has been a Lecturer with the Department of Electrical and Electronic Engineering, Munster Technological University (MTU), Cork, since September 2023. His research interests include integration of electric vehicles, renewable energy systems to electric power grids, and power system operation within the smart grid concept.

BARRY P. HAYES (Senior Member, IEEE) received the Ph.D. degree in electrical power systems engineering from the University of Edinburgh, Edinburgh, U.K., in 2013. He has held a visiting researcher positions with National Grid U.K., U.K., in 2011, and with the University of Tennessee, Knoxville, TN, USA, in 2016. He is currently an Associate Professor in electrical power engineering with University College Cork (UCC), Cork, Ireland, and a Funded Investigator with MaREI, the SFI Research Centre for Energy, Climate and Marine, Cork. Prior to joining UCC, from 2016 to 2018, he was an Assistant Professor with the University of Galway, Galway, Ireland, and from 2013 to 2016, a Marie Skłodowska Curie Research Fellow with IMDEA Energy, Madrid, Spain. His research interests include the electricity grid integration of sustainable energy technologies and the operation and planning of future power systems.